A Multifunctional High-Spin Biradical Pyrazolylbipyridine-bisnitronylnitroxide

ARTICLE *in* ORGANIC LETTERS · JANUARY 2005

Impact Factor: 6.36 · DOI: 10.1021/ol0479040 · Source: PubMed

4 AUTHORS, INCLUDING:

Giorgio Zoppellaro
Palacký University of Olomouc
74 PUBLICATIONS **1,179** CITATIONS
SEE PROFILE

Martin Baumgarten
Max Planck Institute for Polymer Research
279 PUBLICATIONS **4,322** CITATIONS
SEE PROFILE

ORGANIC LETTERS

2004
Vol. 6, No. 26
4929−4932

A Multifunctional High-Spin Biradical Pyrazolylbipyridine-bisnitronylnitroxide

Giorgio Zoppellaro, Volker Enkelmann, Ahmed Geies, and Martin Baumgarten*

Max Planck Institute for Polymer Research, Ackermannweg 10, D-55128, Mainz, Germany

baumgart@mpip-mainz.mpg.de

Received October 10, 2004

ABSTRACT

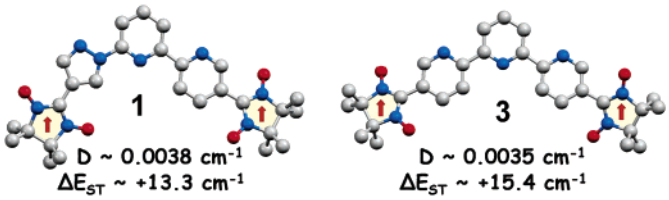

Synthesis and UV–vis, IR, and EPR spectroscopic characterizations, together with X-ray structural analysis, of functional nitronyl- and iminonitroxides attached to pyrazolylbipyridine are described. The exchange interactions between the nitronylnitroxides are found to be stronger than for the iminonitroxides. Although the substitution of a pyridine with the pyrazole ring leads to shorter distances and larger dipolar couplings, the exchange interaction is diminished. While compound 1 forms dimers in the solid state, the terpyridine 3 leads to supramolecular π-stacking.

Various approaches toward magnetic properties or molecular magnets with organic spin units have been dealt with experimentally and theoretically.[1] They can be classified into pure organic ones through synthesis of extended polyradicals or ordering of discrete radical molecules via π-stacking or hydrogen bonding and into the organic inorganic hybrid approach combining organic radicals with spin active metal ions or metal complexes. It has been demonstrated that linear alternating chains of nitronylnitroxides and M(hfac)$_2$ can be formed, even leading to ferro- or ferrimagnetic materials.[2] Therefore, high spin molecules with two or more nitronylnitroxides should not only help to extend the magnetic structures toward higher dimensions but also overcome the usual antiferromagnetic interaction between chains. We now report the synthesis of two such models, the organic biradicals 4″,5′-bis[3-oxide-1-oxyl-4,4,5,5-tetramethyl-imidazoli-din-2-yl]-6-(pyrazol-1″-yl)-2,2′-bipyridine **1** and the 4″,5′-bis[3-oxide-1-oxyl-4,4,5,5-tetramethyl-imidazolin-2-yl]-6-(pyrazol-1″-yl)-2,2′-bipyridine **2**. Because detailed studies of doubly disjoint[3] biradicals are scarce compared with nondisjoint systems,[4] we compare their structure and exchange coupling behavior to the previously reported terpyridines (**3** and **4**)[5] where now also the X-ray structure and the exchange couplings are elucidated (Scheme 1). We experimentally found that despite being doubly disjointed, their estimated through-bond exchange interaction (2J) is both ferromagnetic and unexpectedly large as compared with nondisjointed biradicals, like those based on disemiquinone and dinitroxide systems.[6] The assembly of diradicals **1** and **2** requires the synthesis of the nonsymmetric dicarbaldehyde **9**. This is achieved via a multistep synthetic approach involving Stille coupling of fragments **7** and **8** (Scheme 1)

(1) (a) *Magnetic Properties of Organic Materials*; Lahti, P. M., Ed.; Marcel Dekker: New York, 1999. (b) *Molecular Magnetism*; Kahn, O., Ed.; VCH: Cambridge, U.K., 1993. (c) *Magnetism: Molecules to Materials*; Miller, J. S., Drillon, M., Eds.; Wiley-VCH: Weinheim, 2001−2003; Vols. I−IV.

(2) (a) Caneschi, A.; Gatteschi, D.; Lalioti, N.; Sangregorio, C.; Sessoli, R. *J. Chem. Soc., Dalton Trans.* **2000**, *21*, 3907. (b) Minguet, M.; Luneau, D.; Lhotel, E.; Viller, V.; Paulsen, C.; Amabilino, D. B.; Veciana, J. *Angew. Chem., Int. Ed.* **2002**, *41*, 586.

(3) Matsumoto, T.; Ishida, T.; Koga, N.; Iwamura, H. *J. Am. Chem. Soc.* **1992**, *114*, 9952.

(4) Rajca, A. *Chem. Rev.* **1994**, *94*, 871.

(5) Zoppellaro, G.; Enkelmann, V.; Geies, A.; Baumgarten, M. *Polyhedron* **2003**, *22*, 2099.

(6) (a) Shultz, D. A.; Boal, K. A.; Lee, H.; Farmer, G. T. *J. Org. Chem.* **1999**, *64*, 4386. (b) Shultz, D. A. *Polyhedron* **2001**, *20*, 1627. (c) Shultz, D. A.; Fico, R. M.; Bodnar, S. H.; Kumar, R. K.; Vostrikova, K. E.; Kampf, J. W.; Boyle, P. D. *J. Am. Chem. Soc.* **2003**, *125*, 11761.

10.1021/ol0479040 CCC: $27.50
Published on Web 11/23/2004

Scheme 1

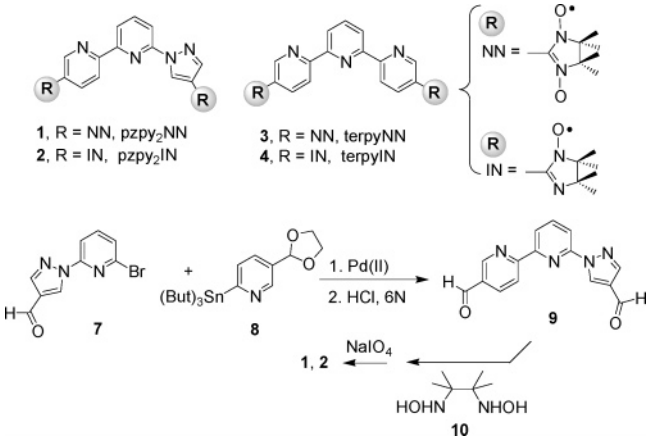

followed by acid hydrolysis of the acetal. Condensation of **9** with bis(hydroxylamino)-dimethylbutane **10** and then by periodate oxidation under phase transfer conditions affords **1** (9%) or **2** (18%) depending on the amount of oxidant used.

The blue nitronylnitroxide biradical **1** ($pzpy_2NN$) is stable as a solid and in toluene solutions. A typical broad band is observed in the visible spectrum (toluene, $\lambda_{max} = 610$ nm, $\epsilon = 1114$ M^{-1} cm^{-1}, $n \rightarrow \pi^*$ transition). Also the orange-red iminonitroxide biradical **2** ($pzpy_2IN$) shows similar stability, with the expected blue-shifted absorption (toluene, $\lambda_{max} = 467$ nm, $\epsilon = 1082$ M^{-1} cm^{-1}). Comparison with the earlier reported aminoxyl-oxide transitions in **3** (toluene, λ_{max} 605 nm, $\epsilon = 480$ M^{-1} cm^{-1})[5] and **4** (toluene, λ_{max} 459 nm, $\epsilon = 380$ M^{-1} cm^{-1})[5] show a hampered radical's optical absorption when the spin carriers are directly bound to the pyridine ring with respect to those directly connected to pyrazole moieties.[7] The IR of **1** features an intense ν_{N-O} stretching vibration at 1352 cm^{-1}, which is weaker and shifted in **2** ($\nu_{N-O} = 1371$ cm^{-1}). These are consistent both in frequency and intensity with those observed in **3**[5] and **4**.[5] Suitable crystals were grown in $CHCl_3$ for **1**[8] and in acetone for **3**.[9] Their structures are reported in Figure 1 together with structural parameters such as dihedral angles (Φ) and intramolecular radical distances. The two systems share nearly planar arrangements of the coupling core and rather small twisting angles between the imidazolyl and the pyridyl/pyrazolyl rings. Therefore, the geometrical prerequisite to enable excellent conjugation between the radical fragments through the coupler is ensured. The biradical **1** forms dimers in the solid state, where

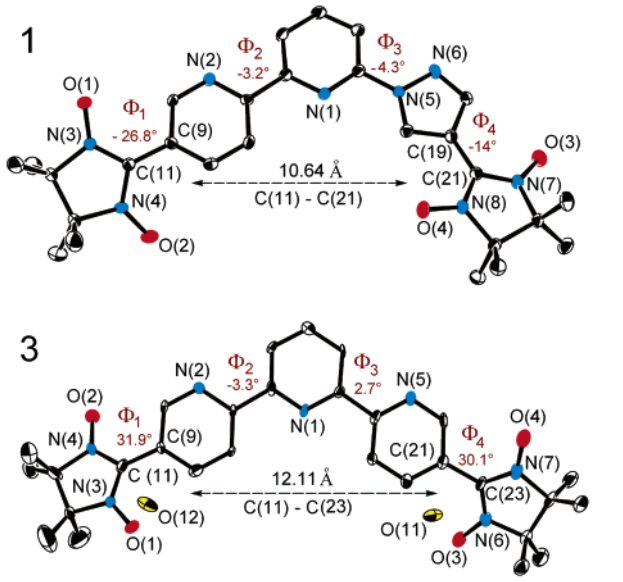

Figure 1. X-ray structures of **1** and **3** with ORTEP drawn at the 50% of the probability level. The hydrogen atoms are omitted for clarity.

inclusion of $CHCl_3$ prevents formation of extended π-networks. The biradical **3**, on the other hand, leads to a supramolecular stacking motif in solid state, with units 180° rotated on top to each at $d \sim 3.3$ Å.

Although such stacking arrangement should give rise to ferromagnetic chains, at 300 K the μ_{eff} value corresponds to 2.44 μ_B, consistent with the theoretical 2.45 μ_B for two uncorrelated spins, hence suggesting the near degeneracy of singlet and triplet states at high temperature. This value remains almost constant down to 70 K; then, it increases weakly, reaching a maximum at ~18 K (2.55 μ_B) followed by a sharp decrease at lower temperatures (Figure 2). The trend in μ_{eff} is analyzed in term of singlet−triplet equilibrium within the molecule, including an averaged intermolecular interaction, θ, adopting the mean-field approximation model.[10]

Such analyses provides a fairly large ferromagnetic through-bond interaction, with $2J/k_b = 29.4 \pm 5.6$ K, and an averaged antiferromagnetic through-space interaction $\theta = -2.6 \pm 0.2$ K (rms = 0.71). To obtain a better estimation of the ΔE_{S-T}, low-temperature EPR studies are then carried out on the dilute toluene solution of **3**. In this way, the

(7) Zoppellaro, G.; Geies, A.; Enkelmann, V.; Baumgarten, M. *Eur. J. Org. Chem.* **2004**, *11*, 2367.

(8) CCDC 229003. Formula for **1**: $C_{28}H_{33}N_8O_4Cl_3$, $M_w = 651.98$, triclinic, space group $P1$ (no. 2), $a = 11.5796(4)$ Å, $b = 12.3160(5)$ Å, $c = 12.7410(5)$ Å, $\alpha = 69.9597(13)°$, $\beta = 65.7760(14)°$, $\gamma = 88.9354(12)°$, $V = 1540.85(11)$ Å^3, $\rho_c = 1.405$ g cm^{-3}, μ (Mo Kα/mm^{-1}) = 0.346, $Z = 2$, $T = 120$ K. Crystal color, shape, and size: blue, prism, 0.09 × 0.21 × 0.38 (mm). Dataset: 31 506 total, 8016 unique reflections ($4.0 < \upsilon < 29.0°$) of which 3793 were observed [$I_0 > 2.0\sigma(I_0)$], N_{ref} 3793, N_{par} 388, $S = 1.07$. The structure was solved by direct methods (SHELXS) and refined by a full-matrix least-squares procedure to R_1 value of 0.0512 ($wR_2 = 0.0571$, all data). The crystallographic data were collected on Nonius Kappa CCD (Mo Kα, $\mu = 0.71073$ Å) diffractometer equipped with a graphite monochromator. The full crystallographic details, excluding structure factors, were deposited with the Cambridge Crystallographic Data Centre.

(9) CCDC 234179. Formula for **3**: $C_{29}H_{37}N_7O_6$, $M_w = 579.66$, monoclinic, space group $P2_1/c$ (no. 14), $a = 6.5690$ Å, $b = 21.5610$ Å, $c = 20.6620$ Å, $\alpha = 90°$, $\beta = 90.8°$, $\gamma = 90°$, $V = 2926.16$ Å^3, $\rho_c = 1.316$ g × cm^{-3}, μ (Mo Kα/mm^{-1}) = 0.094, $Z = 4$, $T = 120$ K. Crystal color, shape, and size: blue, prism, 0.09 × 0.14 × 0.42 (mm). Dataset: 5870 total, 1924 unique reflections ($4.1 < \upsilon < 27.4°$) of which 1911 were observed [$I_0 > 2.0\sigma(I_0)$], N_{ref} 1911, N_{par} 379, $S = 1.07$. The structures were solved by direct methods (SHELXS) and refined by a full-matrix least-squares procedure to R_1 value of 0.0645 ($wR_2 = 0.0666$, all data). The crystallographic data were collected on Nonius Kappa CCD (Mo Kα, $\mu = 0.71073$ Å) diffractometer equipped with a graphite monochromator. The full crystallographic details, excluding structure factors, were deposited with the Cambridge Crystallographic Data Centre.

(10) Bino, A.; Johnston, D. C.; Goshorn, D. P.; Halbert, T. R.; Stiefel, E. I. *Science* **1988**, *241*, 1479.

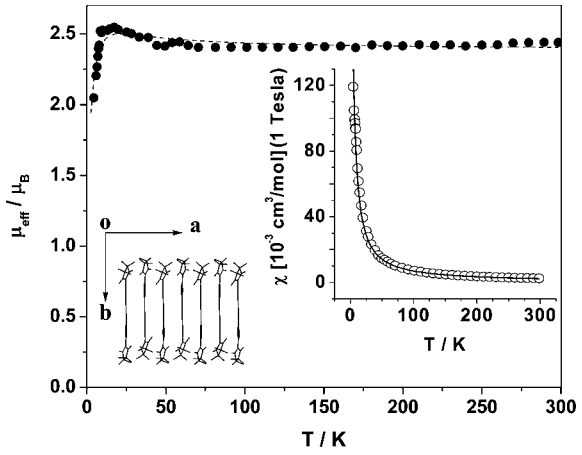

Figure 2. Plot of the observed magnetic susceptibility χ (○) and μ_{eff} (●, units in Bohr magneton μ_B) vs temperature (T, in K) for the crystalline sample of biradical **3**. The inset shows a view down the crystallographic c-axis of a section for the π-stacking of **3**. The best fit curves for μ_{eff} and χ are shown as dashed and plain lines with parameters given in the text.

intermolecular contributions are made negligible (vide infra). The liquid solution EPR spectra (toluene) exhibits 9 lines for **1** (g_{iso} = 2.0066(1)) and 13 lines for **2** (g_{iso} = 2.0061-(1)), confirming the strong exchange coupling ($J \gg a_N$) between the radical fragments. A lower limit of $|J/a_N| \geq 45$ (i.e., $|2J/k_b| \geq 0.06$ cm^{-1}) is extracted upon simulations of their entire EPR envelopes, without, however, gaining knowledge of the sign of J. In frozen solution, the typical zero-field-splitting (zfs) components of $|D/hc| = 3.8 \times 10^{-3}$ cm^{-1} for **1** and $|D/hc| \sim 3.9 \times 10^{-3}$ cm^{-1} for **2** were detected, corresponding to $r \sim 8.8$ and 8.7 Å from a point dipole approach,[11] together with the forbidden $\Delta m_s = 2$ transitions at half field ($g_{av} \sim 4.01$).

At rt and at 120 K, the ratio of double-integrated intensity of the $\Delta m_s = 1$ transitions for **1**−**4** were only 2:1 compared with related monoradicals. Such information already provides the range of energies in which the singlet−triplet gaps are located (0.06 cm^{-1} ≤ $|\Delta E_{S-T}|$ ≤ 83 cm^{-1}). The intensities of the forbidden $\Delta m_s = 2$ signals increased in both **1** and **2** almost linearly upon lowering the temperature down to 4 K (Curie-like). The product DI × T vs T, on the other hand, increased upon lowering the temperature (Figure 3A) for **1**, showing its full triplet occupation. Fitting the DI × T data according to the Bleaney−Bowers model[12] for two interacting $S = 1/2$ systems gave $2J = \Delta E_{S-T} = 13.3 \pm 4.9$ cm^{-1} for **1**. For **2**, the singlet−triplet gap, however, is much smaller and falls in the range of 0.06 cm^{-1} ≤ ΔE_{S-T} ≤ 0.7 cm^{-1} (Figure 3B) with the lower limit being consistent with the rt simulation of its EPR envelope. These findings confirm the greater proclivity of nitronylnitroxides to adopt high-spin ground states compared to iminonitroxides. For the terpyridine biradicals **3** and **4**, careful control of the low-

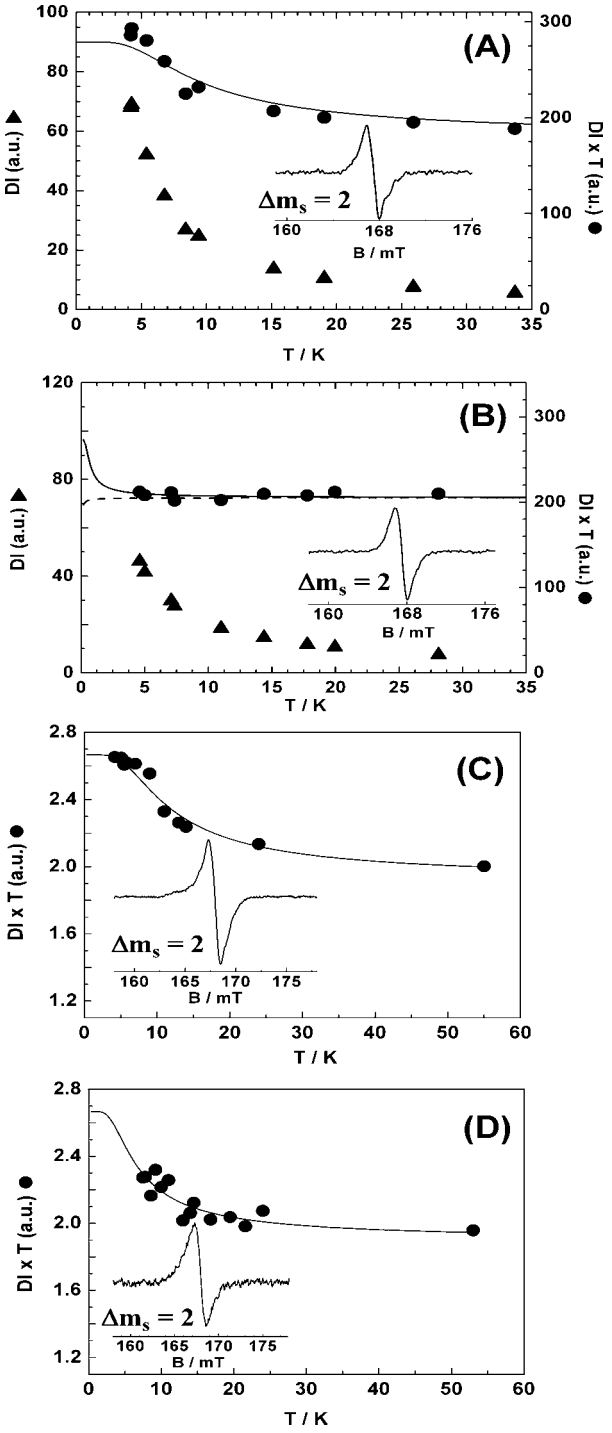

Figure 3. Evolution of the double-integrated signal intensities (DI, ▲) and the product DI × T (●) vs T of the $\Delta m_s = 2$ signal for **1** (**A**), **2** (**B**), **3** (**C**), and **4** (**D**) in the low-temperature range. The solid lines represent the theoretical fitting according to the Bleaney−Bower model, and the insets show the observed $\Delta m_s = 2$ transition at the lowest temperatures (T = 4 K for (**A**), (**B**), and (**C**), T = 7 K for (**D**)). The dashed line in (**B**) shows the fitting assuming the singlet ground state ($S = 0$) and the solid line shows the fitting for the triplet ground state ($S = 1$).

temperature data of the $\Delta m_s = 2$ transitions followed by the DI × T vs T fitting yielded a more accurate ΔE_{S-T} = 15.4

(11) *Electron Paramagnetic Resonance*; Weil, J. A.; Bolton, J. R.; Wertz, J. E., Eds.; VCH−Wiley Interscience: New York, 1994; p 174.
(12) Bleaney, B.; Bowers, K. *Proc. R. Soc. London* **1952**, A214, 451.

$\pm$ 2.0 cm^{-1} for **3** (Figure 3C) and the smaller $\Delta E_{S-T} = 8.7 \pm 1.0$ cm^{-1} for **4** (Figure 3D). Thus, although the shorter distance in pyrazole-containing biradicals **1** and **2** leads to enhanced dipolar couplings (*zfs*) compared to **3** and **4**, the exchange interaction is lowered. This is due to the occurrence of two different pathways for the spin-polarization in **1** and **2**, arising from the presence of a five-membered ring (pyrazole).

In conclusion, we have described new biradicals and compared their structure and exchange interaction, which is sizable and ferromagnetic. In contrast with previous reports in similar pyridine-based nitronylnitroxide biradical systems,[13] where no significant intramolecular interactions are found, the present work shows an efficient propagation of the spin polarization through bond even when a second or a third pyridine ring is introduced as a spacer. Their use in extended networks through their radical units and/or size recognition of their tridentate nitrogen binding cage is presently underway. Such functionalized cores, even without radical units, may further be considered as ligands for promising spin-crossover compounds.[14]

Acknowledgment. Support by the DFG and the Max Planck Society is gratefully acknowledged. The authors thank Prof. W. Haase and Dr. K. Falk (TU Darmstadt) for the magnetic susceptibility measurements.

Supporting Information Available: Detailed synthetic procedures toward biradicals **1** and **2**, ^{1}H, ^{13}C NMR, UV−vis, and IR data, EPR in solution for **1** and **2** (with simulations), in the frozen state and power saturation behaviors for all the radical systems, and X-ray structures of **1**, **3**, and a monoradical (which was used for spin quantization) in CIF format. This material is available free of charge via the Internet at http://pubs.acs.org.

OL0479040

(13) (a) Ziessel, R.; Ulrich, G.; Lawson, R. C.; Echegoyen, L. *J. Mater. Chem.* **1999**, *9*, 1435. (b) Romero, F. M.; Ziessel, R. *Tetrahedron Lett.* **1999**, *40*, 1895. (c) Ziessel, R. *Mol. Cryst. Liq. Cryst.* **1995**, *273*, 101. (d) Stroh, C.; Ziessel, R. *Tetrahedron Lett.* **1999**, *40*, 4543.

(14) Money, V. A.; Evans, I. R.; Halcrow, M. A.; Goeta, A. E.; Howard, J. A. K. *Chem. Commun.* **2003**, 158.

Supporting informations for 10.1021/ol0479040

A Multifunctional high spin biradical pyrazolylbipyridine-bisnitronylnitroxide

Giorgio Zoppellaro, Volker Enkelmann, Ahmed Geies and Martin Baumgarten*
Max Planck Institute for Polymer Research, Ackermannweg 10, D-55128, Mainz, Germany

Content:

General Methods:

Solvents were distilled before use and kept dry over molecular sieves; in particular diethylether and toluene were dried over sodium/benzophenone and distilled under Argon. All the reagents were used as received. ESR spectra were recorded in diluted and oxygen-free solutions of toluene with the concentration of 10^{-4} mol × dm^{-3} unless otherwise stated by using a Bruker X-band spectrometer ESP300 E, equipped with an NMR gaussmeter (Bruker ER035), a frequency counter (Bruker ER 041 XK) and a variable temperature control continuous flow N_2 cryostat (Bruker B-VT 2000) or with Oxford system (ESR 910) helium continuous flow cryostat. The g-factor corrections were obtained by using PNT radical (g = 2.0026) or DPPH (g = 2.0037) as standard. Determination of temperature-dependent magnetic susceptibility of a crystalline sample of **3** was recorded using a Faraday-type balance in a temperature range 4.5–300 K at the applied field **B**=1.0 T. The measurements presented were done using a computer controlled Cahn D-200 microbalance and a Bruker B-MN 200/60 power supply [1]. The diamagnetic correction of the molar magnetic susceptibilities was applied using well-known Pascal's constants [2 and 3]. The corrected magnetic moment has been converted to effective magnetic moment μ_{eff} / μ_B (SI units are employed). The biradicals **1** and **2** were synthesized according to Scheme 1. Two routes towards the carbaldehyde intermediate **7** were tested (Route A and Route B in Scheme 1). Both routes provided comparable yields but the one shown as Route A was somehow faster. The calculation for the spin concentrations of **1, 2, 3** and **4** were carried out on dilute solutions, where the double integrated signal intensities (DI) of the biradicals recorded under non-saturating conditions have been compared against the nitronylnitroxide monoradical (6-bromo-5'[3-oxide-1-oxyl-4,4,5,5-tetramethylimidazolidin-2-yl]-2,2'-bipyridine) **20** for the NN biradicals, and the iminonitroxide monoradical (6-bromo-5'[1-oxyl-4,4,5,5-tetramethylimidazolidin-2-yl]-2,2'-bipyridine) **21** for the INs biradicals. Both **20** and **21** were synthesised according to Scheme 2, and recorded under identical conditions (modulation amplitude, receiver gain, power, sweep time, temperature) using the same EPR tube, and by careful control of the filling factors. In the low temperature EPR experiments for **1**, **2**, **3**, and **4** dilute and degassed solutions have been employed [10^{-3} M in toluene] and the microwave power applied in the measurements were carefully kept in such a way that the signal intensities were proportional to the square root of the power. UV-Vis spectra were recorded in toluene solutions with Perkin Elmer Spectrometer (UV/Vis/NIR Lambda 900) by using 1 cm optical-path quartz cell at room temperature. ^{1}H- and ^{13}C-NMR spectra were recorded on Bruker AMX 250 spectrometer. IR spectra were recorded in KBr pellet (Nicolet 730 FT-IR Spectrometer) at room temperature. Mass spectra were obtained on FD-MS, VG Instuments ZAB-2 mass spectrometer. Elemental

analyses were performed at the University of Mainz, Faculty of Chemistry and Pharmacy on Foss Heraeus Varieo EL. The various melting points (m.p.) were measured on Büchi B-545 apparatus (uncorrected) by using open ended capillaries. The X-ray crystallographic data for the biradicals **1** and **3**, and the monoradical **20** were collected on Nonius Kappa CCD (Mo-Kα) difractometer equipped with graphite monochromator. The structures were solved by direct method (SHELXS) and refined by a full-matrix least-squares procedure. The compounds 6-bromo-3-pyridinecarbaldehyde **11,** 2-bromo-5-[1,3]dioxolan-2-yl-pyridine **10**, 2-tributylstannyl-5-[1,3]dioxolan-2-yl-pyridine **8**, 6-bromo-2,2'-dipyridine-5'-carbaldehyde **18** were prepared according to the full synthetic procedures provided in our previous report [4] and the triformylmethane **15** was prepared according to the other previous report [5]. The 2-bromo-6-hydrazinopyridine **14** was prepared using adapted literature procedures [6] with modifications here described. The 2,3-bis-hydroxylamino-2,3-dimethylbutane **16** (free base) was prepared as described in reference [7]. Compounds **24** and **25** were prepared according to reference [8] with modifications here provided.

References:

[1] Ostrovsky, S.; Haase, W.; Drillon, M.; Panissod, P. *Phys. Rev. B,* **2001**, 64, p. 134418.

[2] Weiss, A.; Witte, H. In: *Magnetochemie*, Verlag Chemie, Weinheim, Germany, **1973**.

[3] Koänig, E. In: Landolt-Boärnstein, Neue Serie Vol. II/2, Springer, Berlin, **1966**, p. 1.

[4] Zoppellaro, G.; Ivanova, A.; Enkelman, V.; Geies, A.; Baumgarten, M. *Polyhedron* **2003**, 22, 2099.

[5] Zoppellaro, G.; Geies, A.; Enkelmann, V.; Baumgarten, M. *Eur. J. Org. Chem*. **2004**, 11, 2367.

[6] Yakhontov, P. *Chem. Heterocycl. Compd.* (English Transl.) **1969,** 5, 851-852.

[7] Ovcharenko, V. I.; Fokin, S. V.; Romanenko, G. V.; Korobkov, I. V.; Rey, P. *Russian Chem. Bulletin* **1999**, 8, 1519.

[8] Vasilevsky, S. F.; Klyatskaya, S.V.; Tretyakov, E.V.; Elguero, J. *Heterocycles*, **2003**, 60 (4), 879.

Scheme 1

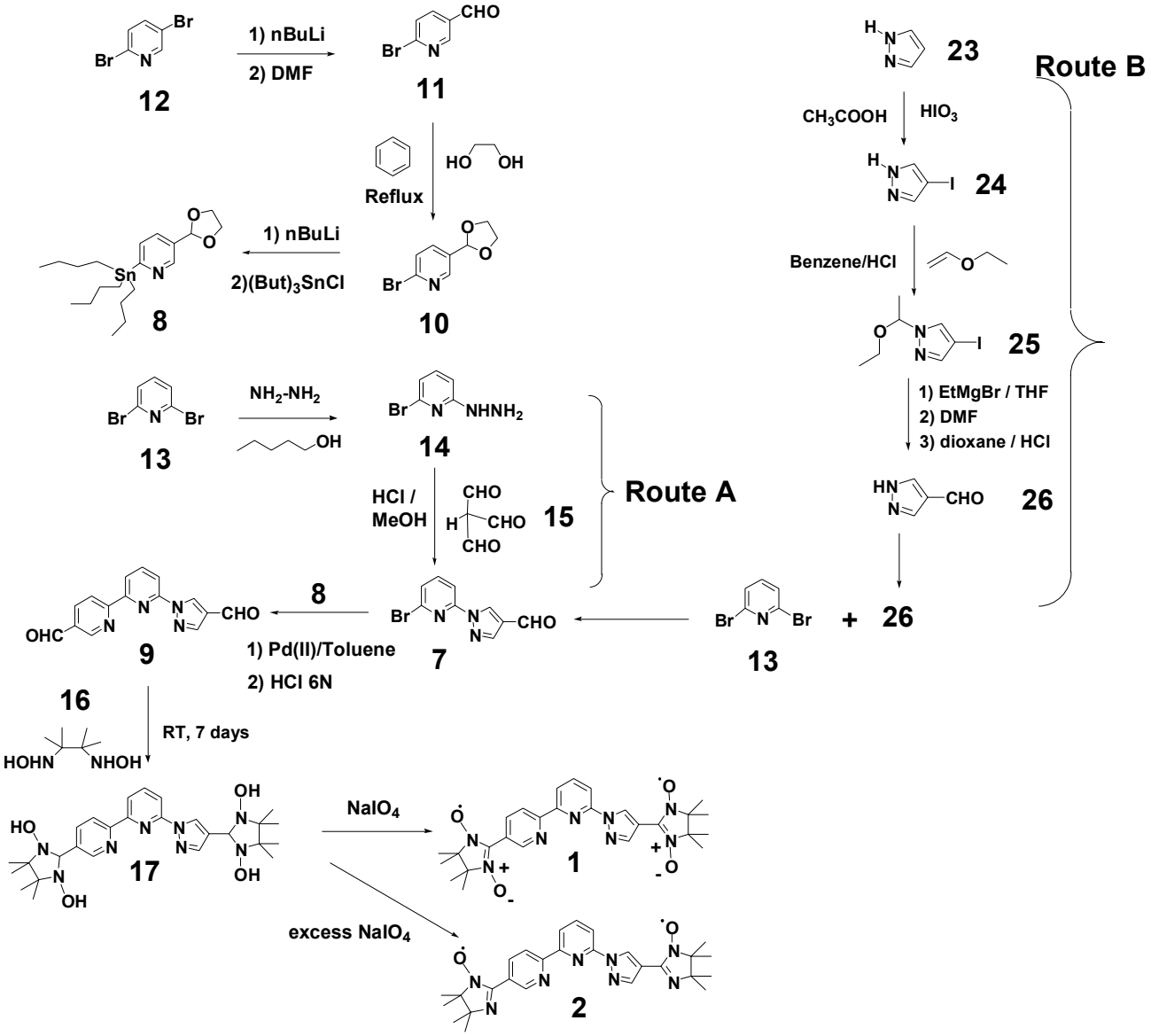

Scheme 2

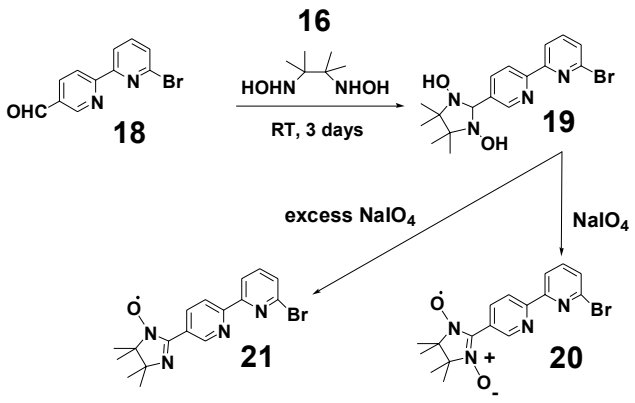

Synthesis of 2-bromo-6-hydrazinopyridine (14) (Route A)

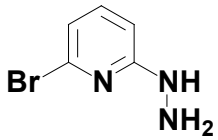

The 2,6-dibromopyridine (**13**, 1.44 g, 6.1 mmol) was charged in a round-bottomed flask together with an excess of hydrazine-monohydrate (1.61 g, 32.2 mmol) and butanol (100 mL) and the mixture was stirred under reflux for 5 hours. Then, the solvent was evaporated slowly under air and yellowish crystals were obtained. The crystals were initially washed with small portions of cold water (3 × 10 mL) then the solid was dissolved in $CHCl_3$. The solution was chromatographed on SiO_2 column ($CHCl_3$/Hexane, 1/2). The unreacted 2,6-dibromopyridine was eluted first (R_f = 0.41) then ethylacetate (EtOAC) was added, and pure 2-bromo-6-hydrazinopyridine was collected as pale yellowish needles after solvent evaporation (0.72 g, yield 63%). Starting from 3 g of 2,6-dibromopyridine (12.66 mmol) and 3.35 g of hydrazine monohydrate (66.92 mmol) it was obtained 1.36 g of 2-bromo-6-hydrazinopyridine **14** (7.23 mmol, yield 57%). **M.p**.117-118°C (from ethylacetate). **FT-IR** (KBr pellet, ν/cm^{-1}): 3307 (m), 3104 (w), 3029 (m), 1564 (s), 1546 (s), 1513 (s), 1385 (s), 1167 (s), 1134 (s), 1093 (s), 980 (s), 787 (s), 742 (s), 650 (s). **MS-FD** (8 kV, CH_2Cl_2) m/z: found 188.1 (100%), $C_5H_6BrN_3$ requires MW 188.03. **^{1}H NMR** (250 MHz, $CDCl_3$, 298 K, 32 scan) δ (ppm): 7.20 (m, -CH), 6.74 (d, ^3J = 7.58 Hz, -CH), 6.61 (d, ^3J= 8.2 Hz, -CH), 6.42 (s, br, -NH-), 3.47 (s, br, -NH_2). **^{13}C NMR** (DMSO-d_6, 63 MHz, 298 K, 1024 scan) δ (ppm): 162.3, 139.6, 139.2, 114.4, 104.5. **UV/vis,** λ_{max} (CH_2Cl_2)/ nm (ε, $mol^{-1} \times cm^{-1}$): 278 (4740), 284 (sh, 3715). **Elemental analyses** found C 31.77, H 3.32, N, 22.21%. $C_5H_6BrN_3$ required C 31.94, H 3.22, N 22.35%.

Synthesis of 6-bromo-2-[4'-formylpyrazol-1'-yl]-pyridine (7) (Route A)

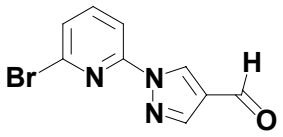

To a mixture of 2-bromo-6-hydrazinopyridine **14** (2.0 g, 10.6 mmol) and triformyl methane **15** (1.06 g, 10.6 mmol) in methanol (60 ml), HCl solution (3.0 mL, 6 N) was added and then stirred for 1 day at room temperature. The solvent was removed under reduced pressure and the residue was neutralized with aqueous Na_2CO_3 solution. The yellowish solid product was

filtered off and dissolved in $CHCl_3$. The mixture was chromatographed on silica gel using mixture of $CHCl_3$/Hexane/Ethylacetate (1/3/1). The yellowish fraction eluted (R_f = 0.67) was collected and upon air-drying it gave pure 6-bromo-2-[4'-formylpyrazol-1'-yl]-pyridine **7** (1.87 g, yield 70%) as pale yellowish powder that strongly retains water. **M.p.**141-142°C. **FT-IR** (KBr pellet, ν/cm^{-1}) 3110 (w, ν_{C-H}), 2865 (m, ν_{C-Hal}), 1668 (s, C=O), 1583(s), 1566 (s), 1544 (s), 1454 (s), 1363 (s), 1211 (s) (pyridine- and pyrazolyl- moieties). **^{1}H NMR** (DMSO-d_6, 250 MHz, 298 K, 16 scan) δ (ppm), 9.96 (s, 1H, -CHO), 9.26 (s, 1H, -CH), 8.31 (s, 1H, -CH), 7.98 (m, 2H, 2-CH), 7.73 (m, 1H, -CH). **^{13}C NMR** (DMSO-d_6, 63 MHz, 298 K, 1024 scan) δ (ppm), 185.4, 149.9, 142.8, 141.5, 139.5, 133.0, 127.1, 125.6, 112.0. **FD-MS** (8 kV, CH_2Cl_2) m/z: found 253.1 (100%), required for $C_9H_7BrN_3O$ (MW+H$^+$) 253.08. **UV/vis**, λ_{max} (CH_2Cl_2)/ nm (ε, mol^{-1} × cm^{-1}): 261 (sh, 11340), 265 (11730), 299 (16350), 338 (broad signal, 685). **Elemental analysis** found C 39.82%, H 3.30%, N 15.20%. $C_9H_6BrN_3O \times H_2O$ required C 40.02, H 2.99, N 15.50%.

Synthesis of 4-iodo-pyrazole (24) (Route B):

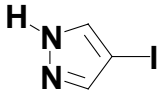

Pyrazole (**23**, 3.4 g, 50 mmol) was dissolved in acetic acid (30 mL) and left under stirring. Separately, a solution containing HIO_3 (1.8 g, 10 mmol), I_2 (5.1 g, 20 mmol), H_2SO_4 (2 mL, 30%) and acetic acid (15 mL) was prepared, leading to a deep red-violet mixture. The pyrazole solution was heated up to 60°C under argon, and then the iodine mixture was slowly added, taking care that before any further addition, all the iodine was consumed. When half of the addition was completed, the rest of the iodine was dropped fully, and the pyrazole solution was left to react for 60 min. Then, a saturated solution of $NaHCO_3$ (15 mL) was added in order to smoothly start the quenching of the acetic acid. A saturated solution of Na_2CO_3 was finally added slowly until no evolution of CO_2 was observed and a fine white flocculate was formed. The flocculate was extracted with $CHCl_3$ (3 × 30 mL), the organic layer dried over $MgSO_4$, filtered and left to crystallise under air. Finally 8.6 g as white needles of 4-iodo-pyrazole (**24**) have been obtained (yield 88%).

M.p. 107-108°C (from $CHCl_3$) (literature M.p. 108.5°C). **^{1}H NMR** (250 MHz, $CDCl_3$, 298 K, 16 scan), δ (ppm): 9.51 (s, broad, 1H, -NH), 7.62 (s, asymmetric, 2H, 2-CH). **^{1}H NMR** (250 MHz, DMSO-*d_6*, 298 K, 16 scan), δ (ppm): 13.20 (s, broad, 1H, -NH), 7.90 (s, broad, 1H, -

CH), 7.62 (s, broad, 1H, -CH). **^{13}C NMR** (DMSO-d_6, 63 MHz, 256 scan), δ (ppm): 56.9, 133.6, 143.8. **FT-IR** (KBr): ν/cm^{-1} = 3114 – 2788 (m, several broad vibronic band), 1624 (m), 1537 (m), 1475 (m), 1452 (m), 1365 (s), 1328 (m), 1267 (m), 1178 (m), 1141 (m), 1033 (s), 954 (s), 937 (vs), 871 (s), 810 (vs), 609 (vs). **FD-MS** (8 kV, $CHCl_3$) m/z: found 194.1 (100%), requires for $C_9H_7BrN_3O$ (MW+H^+) 193.97. **Elemental analyses**, found C 18.40, H 1.62, N 14.32. $C_3H_3N_2I$ (193.97) required C 18.58, H 1.56, N 14.44%.

Synthesis of 1-(1-ethoxyethyl)-4-iodo-pyrazole (25) (Route B):

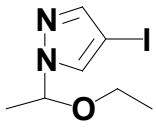

Into a 4-iodo-pyrazole (**24**, 3.0 g, 15.47 mmol, 1 eq.) solution, previously dissolved in 20 mL of benzene, were added 3 drops of HCl (33%,v/v) and ethylvinylether (ethoxyethene, 2.0 mL, d = 0.754 g/mL, 21 mmol, 1.36 eq.) and left under stirring for 6 hours at 45-50°C. A bright yellow-orange solution was slowly formed. The solution was cooled to room temperature and neutralised with a saturated solution of $NaHCO_3$ in water. Then the organic phase was separated and the water phase extracted with portions of benzene (3 × 10 mL). The collected organic portions were dried over $MgSO_4$ and reduced to small volume. The crude mixture was chromatographed on Al_2O_3 column using a mixture of hexane/$CHCl_3$/etylacetate (2/4/1). The first fraction eluted (R_f = 0.75) was concentrated under reduced pressure (60°C, 20 mbar) and 1-(1-ethoxyethyl)-4-iodo-pyrazole (**25**) was collected highly pure (3.9 g, 4.2 mL, 3.49 mmol/mL, yield 94.7 %) as very pale yellowish oil.

^{1}H NMR (250 MHz, $CDCl_3$, 298 K, 16 scan), δ (ppm): 7.61 (s, 1H, -CH), 7.47 (s, 1H, -CH), 5.49-5.42 (q, ^{3}J = 6 Hz, 2H, -CH), 3.48-3.23 (m, 2H, -CH_2), 1.60 (d, ^{3}J = 6 Hz, 3H, -CH_3), 1.11 (t, ^{3}J = 7 Hz, 3H, -CH_3). **^{13}C NMR** ($CDCl_3$, 63 MHz, 298 K, 256 scan), δ (ppm): 14.7, 22.1, 57.3, 64.2, 87.9, 130.6, 143.7. **FD-MS** (8 kV, CH_2Cl_2) m/z: found 266.1 (100%), requires for $C_7H_{11}IN_2O$ (MW+H^+) 266.08.

Synthesis of 4-formyl-1(H)-pyrazole (26) (Route B)

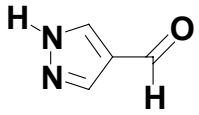

In a small round bottomed flask (20 mL) closed at the top with a rubber cup, it was placed 1-(1-ethoxyethyl)-4-iodo-pyrazole (**25**) (1.5 mL, 5.2 mmol) and THF (6 mL), then the solution was cooled in ice bath (0-4°C), carefully evacuated and kept under argon. A cold solution of EtMgBr (Grignard reagent, CH_3CH_2MgBr, 1.9 mL, 5.7 mmol) was slowly added drop by drop with a syringe through the rubber septum into the cold solution of iodo-pyrazole within 5 min. A milky solution that became a solid paste was slowly formed due to the low solubility of the pyrazolyl-magnesiate derivative. The solution was then aged under stirring for 60 min. Dry DMF (0.5 mL, d = 0.946 g/mL, 6.5 mmol) was added drop by drop while keeping the temperature below 4°C, and left under stirring for 60 min. Then the ice bath was removed and left at room temperature for 30 min.

A pale yellowish solution very dense was formed. A saturated solution of NH_4Cl (5 mL) was added, left under stirring for 20 min, and the organic layer collected, while the water phase was extracted with portions of $CHCl_3$ (3 × 10 mL). The organic phases were collected and allowed to dry under stream of air affording pale yellowish oil. This oil, that contained the aldehyde still protected with the ethoxyethyl-group (TLC SiO_2, ethylacetate/$CHCl_3$/ hexane, 1/4/2, R_f = 0.5-0.7), was placed in a flask together with dioxane (10 mL) and HCl (10 mL, 20% in water) and left under stirring at 60 °C overnight. The solution was neutralised with a saturated solution of K_2CO_3 in water, and the water phase extracted with ethylacetate (3 × 10 mL).

The organic phases were collected, reduced to a small volume and chromatographed over a small SiO_2 column (ethylacetate/ hexane, 1/2), and pure 4-formyl-1(H)-pyrazole (**26**) (R_f = 0.2) as been collected as very sticky yellowish powder (0.4 g, yield 80%). The spectroscopic data of this compound were published in our previous work (see Reference [5]).

Synthesis of 6-bromo-2-[4'-formylpyrazol-1'-yl]-pyridine (7) (Route B)

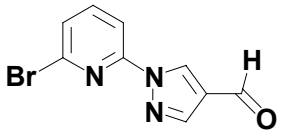

To a solution of 4-formylpyrazole **26** (0.5 g, 5.2 mmol) dissolved in dry THF (30 mL), potassium metal was added (0.2 g, 5.2 mmol) then the mixture was heated to reflux in argon (~ 70 °C) under stirring until all of the potassium was reacted to form the pyrazolate-derivative. Then, 2,6-dibromopyridine **13** (1.14 g, 4.8 mmol) was added and the reaction mixture was left at 70 °C for further 60 h under argon. Then, upon cooling, the THF was evaporated under reduced pressure. The residue was washed with water and the solid yellowish powder was collected, dissolved in $CHCl_3$ and chromatographed on silica (SiO_2) using a mixture of $CHCl_3$/Hexane/Ethylacetate (1/3/1). Pure **7** was then collected (R_f = 0.67, 0.76 g, yield 60%). For the spectroscopic data of **7** see previous page S7 (Route A).

Synthesis of 4'',5'-diformyl-6-(pyrazol-1''-yl)-2,2'-bipyridine (9)

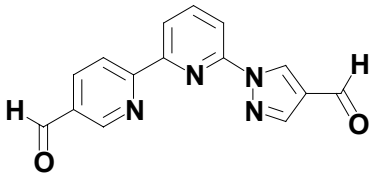

The 2-tributylstannyl-5-[1,3]dioxolan-2-yl-pyridine **8** (3.8 ml, 4.7 mmol) was placed in a two-necked round bottomed flask together with the 6-bromo-2-[4'-formylpyrazol-1'-yl]pyridine **7** (720 mg, 2.8 mmol). The mixture was degassed and kept under rigorous argon atmosphere. Then dry and degassed toluene (30 mL) was added with a syringe together with dichlorobis(triphenylphosphine)-palladium(II) (296 mg, 0.42 mmol), triphenylphosphine (220 mg, 0.84 mmol) and catalytically amount of CuI (20 mg, 0.1 mmol). The solution was then heated to reflux in argon atmosphere under stirring for 60 hours. The very dark solution resulting was filtered from the inorganic salts, collected and washed with a saturated solution of ammonium-chloride (20 mL). The mixture was shaken vigorously in a separator funnel. The aqueous layer was extracted with toluene (2 × 15 mL) and the combined dark organic layers were collected and the solvent evaporated under reduced pressure. The oily solution was treated with HCl (20 mL, 6N) and heated to reflux for 8 hours under stirring; this ensures for the complete hydrolysis of the dioxolane. Basification with saturated solution of potassium carbonate K_2CO_3 shows the formation of a yellowish flocculate at pH = 8 that

consists of the product **9**. The product was extracted with dichloromethane (3 × 20 mL). The organic layers were collected and the solvent evaporated to small volume under reduced pressure to afford a yellowish powder. The product was further washed with small portions of light petroleum ether (2 × 10 ml) (b.p. 30 - 40°C) and 4",5'-diformyl-6-(pyrazol-1"-yl)-2,2'-bipyridine **9** was collected analytically pure as yellowish powder that strongly retains water (360 mg, yield 46 %).

M.p. 221 - 222°C. **FT-IR** (KBr pellet, ν/cm^{-1}) 3128 (w, ν_{C-H}), 2946 (w, ν_{C-H}), 2915 (w, ν_{C-H}), 2848 (w, ν_{C-H}), 1689 (s and asymmetric, C=O), 1592(s), 1546 (s), 1463 (s), 1454 (s), 1363 (s), 1211 (s) (pyridine- and pyrazolyl- moieties).**^{1}H NMR** (DMSO-d_6, 250 MHz, 298 K, 64 scan) δ (ppm), 10.20 (s, 1H, -CHO), 10.01 (s, 1H, -CHO), 9.70 (s, 1H,-CH), 9.22 (s, 1H, CH), 8.88 (d, ^{3}J = 8.16 Hz, 1H, -CH), 8.47 (m. 2H, 2-CH), 8.36 (s, 1H, -CH), 8.26 (t, ^{3}J = 7.85 Hz, 1H, -CH), 8.11 (d, ^{3}J = 7.84 Hz, 1H, -CH). **^{13}C NMR** (DMSO-d_6, 63 MHz, 298 K, 8000scan) δ (ppm): 192.1, 185.3, 158.0, 153.1, 151.4, 149.7, 141.6, 141.4, 137.40, 132.6, 131.5, 125.5, 121.4, 120.6, 114.0. **MS-FD** (8 kV, CH_2Cl_2) m/z: found 278.30 (100%), $C_{15}H_{10}N_4O_2$ required MW. 278.27. **Elemental analyses**, found C 60.50; H, 4.23; N, 18.67%. $C_{15}H_{10}N_4O_2 \times H_2O$ required C 60.81, H 4.08, N 18.91%. **UV/vis** (DMSO) λ_{max} (ε, mol^{-1} × cm^{-1}) 320 nm (17230).

Synthesis of 4",5'-bis[1,3-dihydroxy-4,4,5,5-tetramethylimidazolidin-2-yl]-6-(pyrazol-1"-yl)-2,2'-bipyridine (17)

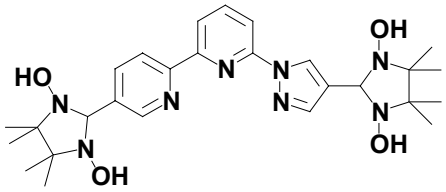

The 4",5'-diformyl-6-(pyrazol-1"-yl)-2,2'-bipyridine (**9**, 180 mg, 0.65 mmol) was placed in a round bottomed flask together with 2,3-bis-hydroxylamino-2,3-dimethylbutane (**16**, 337 mg, 2.27 mmol). A mixture of 1,4-dioxane and trichloromethane (10 mL/10 mL) was used as reaction solvents due to the low solubility of **9**. The mixture was then stirred for 7 days under argon at room temperature. The solution appeared yellowish-orange with no hint of precipitate formation. Afterwards the mixture was dried under air and a pale brownish powder was obtained that it was washed on filter paper with small portions of cold water (2 × 5 mL) and cold light petroleum ether (2 × 5 mL). Finally 255 mg of crude 4",5'-bis[1,3-dihydroxy-4,4,5,5-tetramethylimidazolidin-2-yl]-6-(pyrazol-1"-yl)-2,2'-bipyridine **17** as light brown

powder was obtained (yield of the crude 73%). A complex ^{1}H-NMR (250 MHz, DMSO-d_6) indicated that the residue was a mixture of the desired product **17**, plus the excess of 2,3-bis-hydroxylamino-2,3-dimethylbutane and its decomposition products (oxime). Nevertheless, it was judged adequate for the next oxidation step**. M.p.** 213-214°C. **FT-IR** (KBr pellet, ν/cm^{-1}) 3257 (s, broad, -OH), 2977 (s, $\nu_{C\text{-}Hal}$), 2925 (s, $\nu_{C\text{-}Hal}$), 2859 (s, $\nu_{C\text{-}Hal}$), 1594 (s), 1563 (m), 1465 (s) (pyridyl and pyrazolyl-moieties), 1386 (s), 1141 (s and wide).

Synthesis of 4'',5'-bis[3-oxide-1-oxyl-4,4,5,5-tetramethylimidazolin-2-yl]-6-(pyrazol-1''-yl)-2,2'-bipyridine (1)

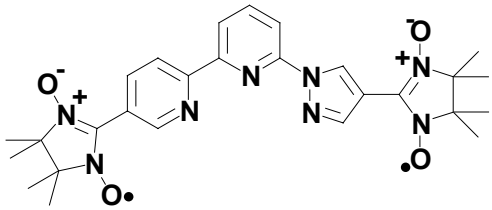

The crude 4'',5'-bis[1,3-dihydroxy-4,4,5,5-tetramethylimidazolidin-2-yl]-6-(pyrazol-1''-yl)-2,2'-bipyridine **17** (130 mg, 0.24 mmol) was charged into a small flask together with $CHCl_3$ (15 mL), degassed and kept under argon while stirring at room temperature. Separately, a solution of $NaIO_4$ (128 mg, 0.6 mmol) dissolved in water (15 mL) was degassed and saturated by argon exchange; then it was added to the solution of the radical precursor by using a syringe under argon. After 20 min a deep blue-violet solution was obtained. The organic layer was extracted by using portions of $CHCl_3$ (3 × 10 mL) until the aqueous phase was almost colourless. The organic solution was evaporated by continuous argon bubbling till small volume. The mixture was separated by column chromatography (Aluminium oxide, Al_2O_3, acetone/light petroleum ether, 1/3) where seven different fractions were collected (Aluminium oxide, acetone/light petroleum ether, 1/3). The 4'',5'-bis[3-oxide-1-oxyl-4,4,5,5-tetramethylimidazolin-2-yl]-6-(pyrazol-1''-yl)-2,2'-bipyridine **1** (R_f = 0.37) was obtained after solvent evaporation as deep blue powder in poor yield (12 mg, yield 9 %).

M.p. 209 – 210°C (from acetone). **FT-IR** (KBr pellet, ν/cm^{-1}): 3174 (w, $\nu_{C\text{-}H}$), 3097 (w, $\nu_{C\text{-}H}$), 2983 (m, $\nu_{C\text{-}H}$), 2937 (w, $\nu_{C\text{-}H}$), 2869 (w, $\nu_{C\text{-}H}$), 1592 (s), 1548 (m), 1462 (s), 1423 (m), 1387 (m), 1352 (s, N-O), 1217 (m). **UV/vis**, λ_{max} (toluene)/ nm (ε, mol^{-1} × cm^{-1}): 321 (33624), 336 (35017), 350 (31867), 373 (17510), 392 (10685), 470 (163), 518 (260), 564 (634), 610 (1114), 666 (1004), 746 (70). **Elemental analyses** found C 60.64, H 6.01, N 20.84 (%).$C_{27}H_{32}N_8O_4$ required C 60.89, H 6.06, N 21.04%. **EPR** (298 K, 10^{-4} M toluene): 9 lines, g_{iso} = 2.0066(1).

Synthesis of 4'',5'-bis[-1-oxyl-4,4,5,5-tetramethylimidazolin-2-yl]-6-(pyrazol-1''-yl)-2,2'-bipyridine (2)

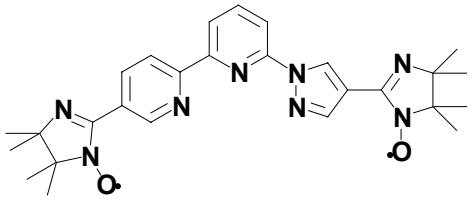

The compound **17** (125 mg, 0.23 mmol) was charged into a small flask and dissolved in $CHCl_3$ (15 mL). Then a solution of $NaIO_4$ (197 mg, 0.92 mmol) dissolved in water (15 mL) was added. After 40 min a deep orange-red solution was obtained. The organic layer was extracted by using portions of $CHCl_3$ (3 × 10 ml) until the aqueous phase was almost colourless. The organic solution was evaporated under reduced pressure till small volume. The mixture was separated by column chromatography (Aluminium oxide, acetone/hexane, 2/3) were four different fractions have been collected. The 4'',5'-bis[-1-oxyl-4,4,5,5-tetramethylimidazolin-2-yl]-6-(pyrazol-1''-yl)-2,2'-bipyridine **2** (R_f = 0.42) was obtained after solvent evaporation as fine orange-red powder, that was further recrystallised from $CHCl_3$ (21 mg, yield 18%).

M.p. 205 – 206°C (from $CHCl_3$). **FT-IR** (KBr pellet, ν/cm^{-1}): 3160 (w, ν_{C-H}), 3104 (w, ν_{C-H}), 2977 (m, ν_{C-H}), 2929 (m, ν_{C-H}), 2865 (m, ν_{C-H}), 1595 (s), 1458 (vs), 1409 (m), 1371 (s, N-O), 1267 (m) 1157 (m) (pyridine and pyrazolyl moieties). **UV/vis**, λ_{max} (toluene)/nm (ε, mol^{-1} × cm^{-1}): 321 (26100), 417 (791), 442 (997), 467 (1082), 496 (773), 536 (284). **Elemental analyses** found C 61.74, H 6.10, N 20.97%. $C_{27}H_{32}N_8O_4$ × ⅓ $CHCl_3$ required C 62.07, H 6.23, N 21.19. **EPR** (298 K, 10^{-4} M toluene): 13 lines, g_{iso} = 2.0061(1).

Synthesis of 6-bromo-5'[1,3-dihydroxy-4,4,5,5-tetramethylimidazolidin-2-yl]-2,2'-bipyridine (19)

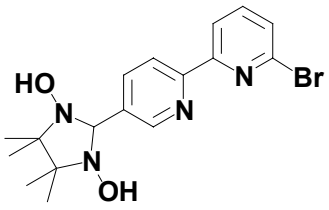

A mixture of 6-bromo-2,2'-dipyridine-5'-carbaldehyde **18** (280 mg, 1.06 mmol) and 2,3-bis(hydroxylamino)-2,3-dimethylbutane **16** (444 mg, 3.0 mmol) were dissolved in 30 mL of a mixture of dioxan and CH_2Cl_2 (1/1) and stirred under argon for four days until a fine white

precipitate was formed. The solvent was removed by slow evaporation at room temperature and the solid product was collected, washed with a small amount of cold methanol/water mixture (1/1), and air dried to give crude **19** (354 mg, crude yield 85 %) that was subjected to the oxidation step without further purification.

It decomposes before melting (from white powder to bright red powder) at 166-167 °C (from methanol). **FT-IR** (KBr pellet, ν/cm^{-1}) 3251 (s and very broad, -OH), 2983 (s, ν_{C-H}), 2920 (s, ν_{C-H}), 1570 (m), 1548 (m), 1431 (s), 1378 (s), 1255 (w), 1155 (s), 1124 (s), 875 (s) 790 (s). **^{1}H NMR** (DMSO-d$_6$, 250 MHz) δ (ppm) 8.65 (s, 1H, -CH), 8.31 (d, ^3J = 7.53 Hz, -CH), 8.18 (d, ^3J = 8.17, 1H, -CH), 7.96-7.92 (dd, ^3J = 8.16 Hz, 1.9 Hz,1H, -CH), 7.87 (s, 1H, -OH), 7.82 (t, ^3J = 7.85 Hz, 1H, -CH), 7.62 (d, ^3J = 7.54 Hz, 1H, -CH), 4.56 (s, 1H, -CH$_{imid}$), 1.00 (d, ^3J = 7.84 Hz, 12 H, 4-CH$_3$). **^{13}C NMR** (63 MHz, DMSO-d$_6$) δ (ppm): 156.7, 152.7, 149.7, 149.4, 141.0, 140.6, 138.3, 137.2, 128.2, 119.7, 87.8, 66.3, 24.2, 17.2. **Elemental analyses** found C 47.76, H 5.75, N, 12.81%. $C_{17}H_{21}BrN_4O_2 \times 2\ H_2O$ (429.31) required C 47.56, H 5.87, N 13.05.

Synthesis of 6-bromo-5'[3-oxide-1-oxyl-4,4,5,5-tetramethylimidazolidin-2-yl]-2,2'-bipyridine (20)

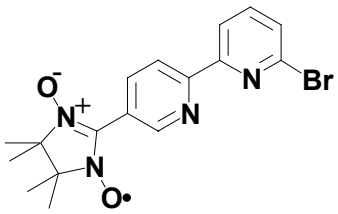

The 6-bromo-5'[1,3-dihydroxy-4,4,5,5-tetramethylimidazolidin-2-yl]-2,2'-bipyridine **19** (250 mg, 0.58 mmol) was oxidized under phase transfer conditions in water/chloroform mixture (30mL, 1/3) using $NaIO_4$ (186 mg, 0.87 mmol) for 30 min; during this period of time the color gradually changed to give finally a blue-green organic solution. The phases were separated and the aqueous layer was extracted with chloroform (3 × 15 mL). The organic phases were collected and evaporated under air. The green-blue solid was dissolved in the minimum amount of acetone and chromatographed on neutral alumina using a mixture of acetone/petroleum-ether (low boiling point, 1/3) as eluents. The first blue fraction eluted was collected and the solvent was removed under reduced pressure to afford pure 6-bromo-5'[3-oxide-1-oxyl-4,4,5,5-tetramethylimidazolidin-2-yl]-2,2'-bipyridine **20** (56 mg, yield 25 %) as deep blue powder.

M.p. 165 – 166 °C (from acetone). Upon melting changes from deep-blue to bright orange. **FT-IR** (KBr pellet, ν/cm^{-1}) 3112 (w, ν_{C-H}), 2981 (s, ν_{C-H}), 2933 (s, ν_{C-H}), 2875 (s, ν_{C-H}), 1583 (m), 1548 (m), 1454 (s), 1430 (s), 1413 (s), 1352 (s, N-O), 1213 (m), 1124 (m) (pyridine and pyrazolyl- moieties). **UV/vis**, λ/nm (toluene), (ε, M^{-1}× cm^{-1}): 316 (23270), 327 (24480), 342 (20235), 377 (5580), 394 (8960), 468 (84), 498 (71), 537 (115), 574 (187), 620 (259), 669 (221), 746 (65). **Elemental analyses** found C 47.76, H 5.45, N 12.90%. $C_{17}H_{18}BrN_4O_2$ × $2H_2O$ (425.08) required C 47.90, H 5.20, N 13.14%. **EPR** (298 K, 8 × 10^{-5} M in toluene): five lines, g_{iso} = 2.0066(1), a_N = 0.748 mT.

Synthesis of 6-bromo-5'[1-oxyl-4,4,5,5-tetramethylimidazolidin-2-yl]-2,2'-bipyridine (21)

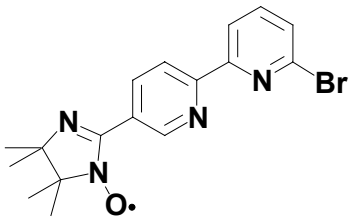

The 6-bromo-5'[1,3-dihydroxy-4,4,5,5-tetramethylimidazolidin-2-yl]-2,2'-bipyridine **19** (100 mg, 0.23 mmol) was oxidized under phase transfer conditions in water/chloroform mixture (20 mL, 1/3) using excess of $NaIO_4$ (242 mg, 1.63 mmol), previously dissolved in 15 mL of water, for 60 min and upon warming the reaction mixture up to 40°C. During this period of time the color gradually changed to give a bright red organic solution. The phases were separated and the aqueous layer was extracted with chloroform (3 x 20 mL). The organic phases were collected and evaporated under reduced pressure. The crude red solid was dissolved in acetone and purified by chromatographic separation on neutral alumina, using acetone /petroleum ether (low boiling point, 1/3) mixture as eluents. The red fraction eluted (R_f = 0.67) was collected and upon drying it gave pure 6-bromo-5'[1-oxyl-4,4,5,5-tetramethylimidazolidin-2-yl]-2,2'-bipyridine **21** (24 mg, yield 28 %) as very hygroscopic bright red solid. **M.p.**147 – 148°C (from acetone). **FT-IR** (KBr pellet, ν/cm^{-1}) 3072 (w, ν_{C-H}), 2964 (s, ν_{C-Hal}), 2923 (s, ν_{C-H}), 2855 (s, ν_{C-H}), 1594 (m), 1544 (s), 1455 (m), 1428 (s), 1374 (s, N-O), 1261 (m), 1155 (s), 1124 (s) (pyridine and pyrazolyl- moieties). **UV/vis**, λ/nm (toluene)/nm (ε, M^{-1} × cm^{-1}) 308 (19086), 343 (3222), 392 (282), 438 (278), 464 (321), 493 (287), 534 (157). **Elemental analyses** found C 47.43, H 5.85, N, 13.00%. $C_{17}H_{18}BrN_4O$ × 3 H_2O (428.30) required C 47.67, H 5.65, N 13.08. **EPR** (298 K, 10^{-4} M in toluene): seven lines, g_{iso} = 2.0061(1), a_{N1} = 0.885 mT, a_{N2} = 0.430 mT.

^{1}H and ^{13}C NMR data

Figure S1. ^{1}H NMR ($CDCl_3$, 250 MHz, 298 K, 64 scans) of 6-bromo-3-pyridinecarbaldehyde (11)

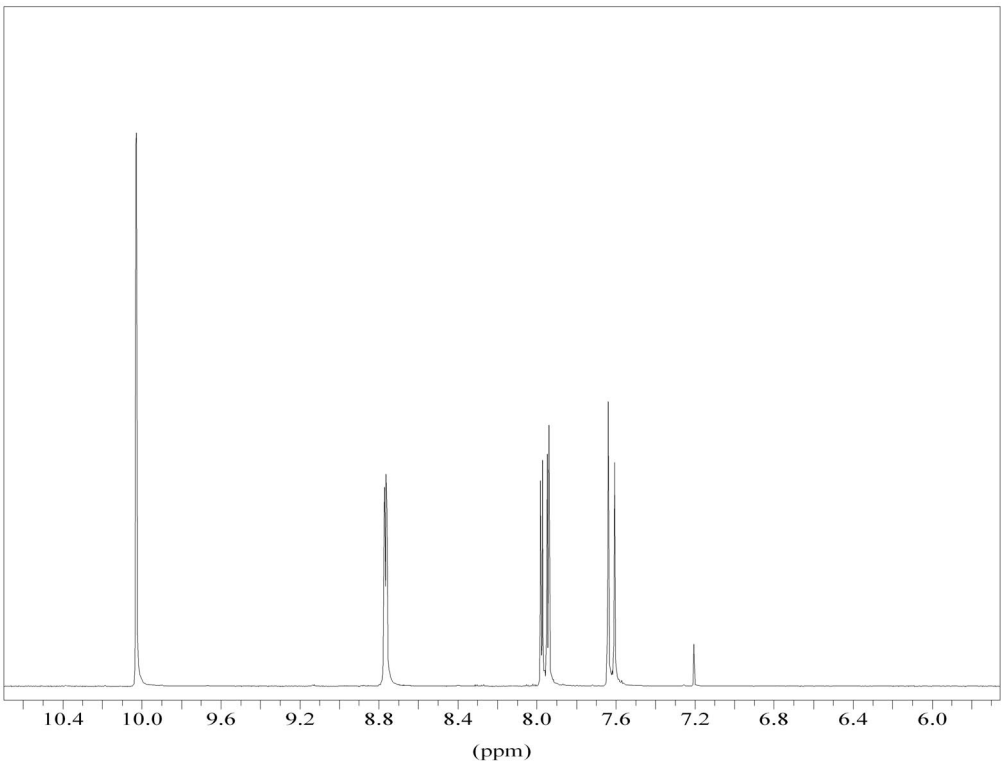

Figure S2. ^{13}C NMR ($CDCl_3$, 250 MHz, 298 K, 10000 scans) of 6-bromo-3-pyridinecarbaldehyde (11)

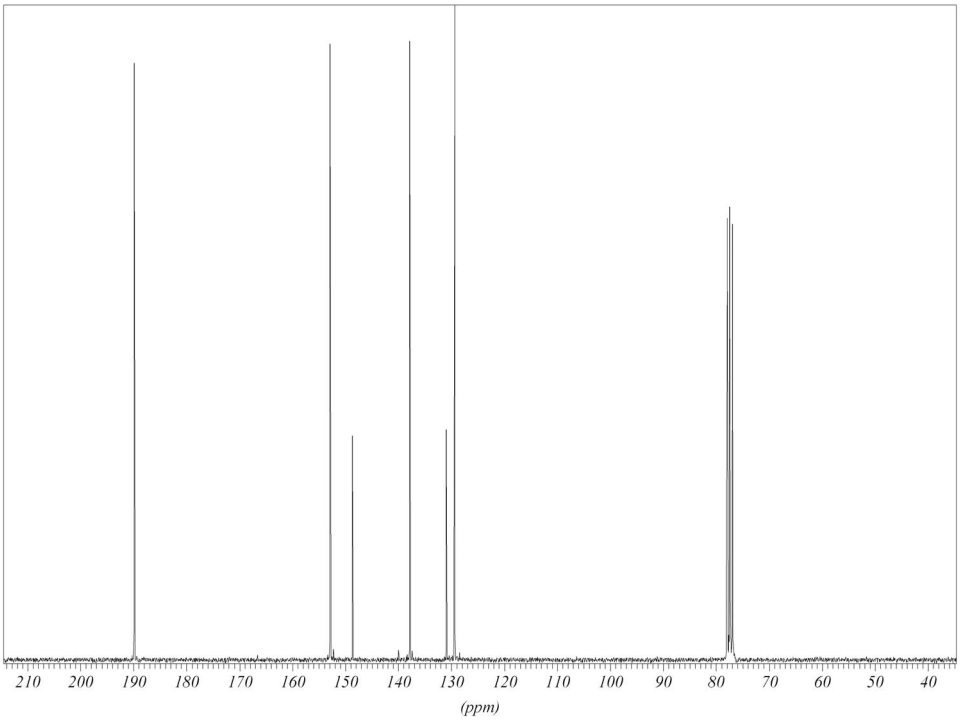

Figure S3. ^{1}H NMR ($CDCl_3$, 250 MHz, 298 K, 16 scans) of 2-bromo-5-[1,3]dioxolan-2-yl-pyridine (10)

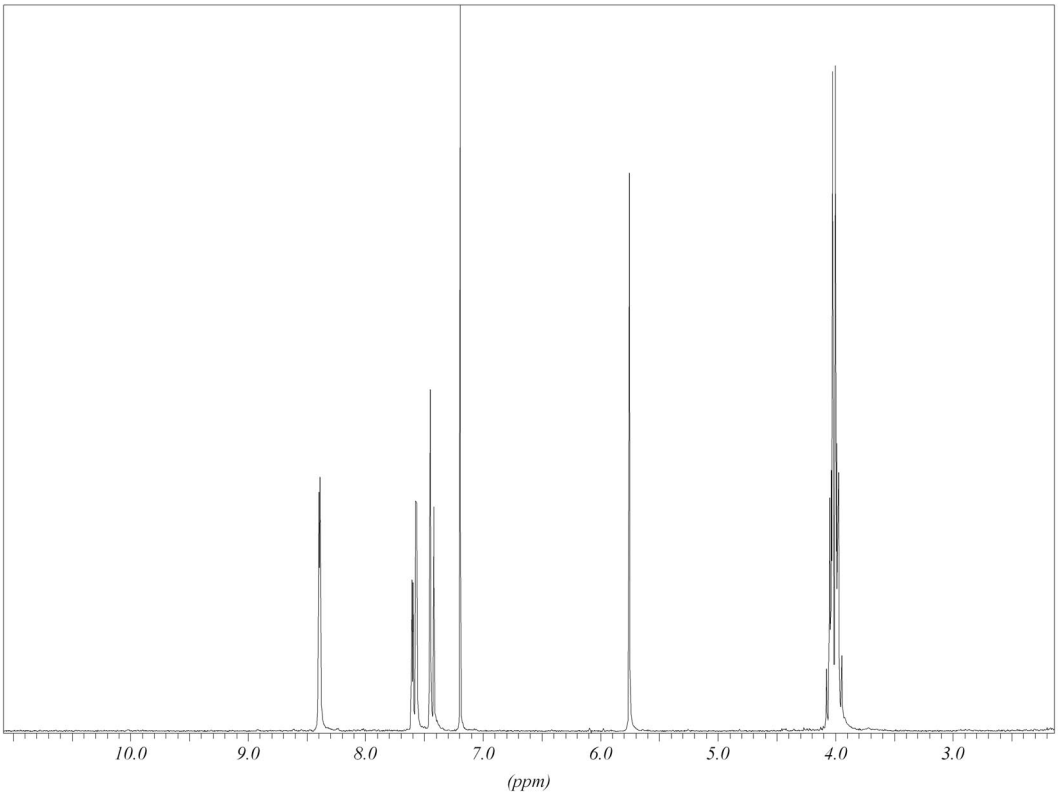

Figure S4. ^{13}C NMR ($CDCl_3$, 63 MHz, 298 K, 9000 scans) of 2-bromo-5-[1,3]dioxolan-2-yl-pyridine (10)

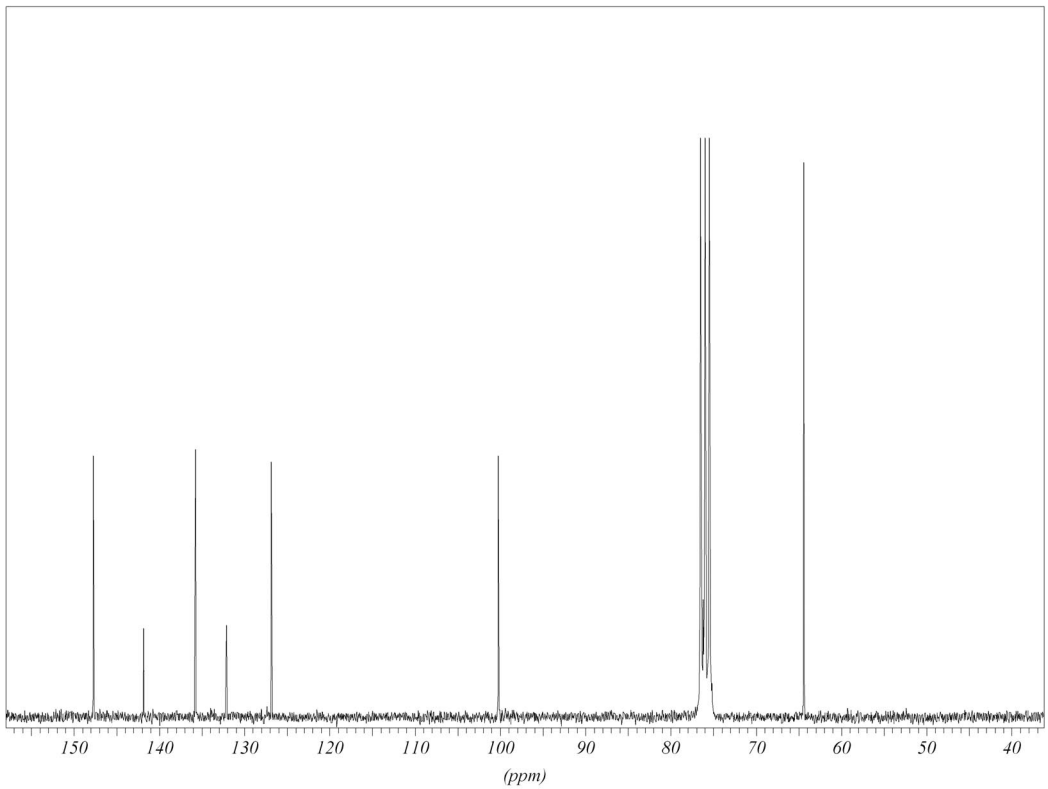

Figure S5. ^{1}H NMR ($CDCl_3$, 250 MHz, 298 K, 16 scans) of 2-bromo-6-hydrazinopyridine (14)

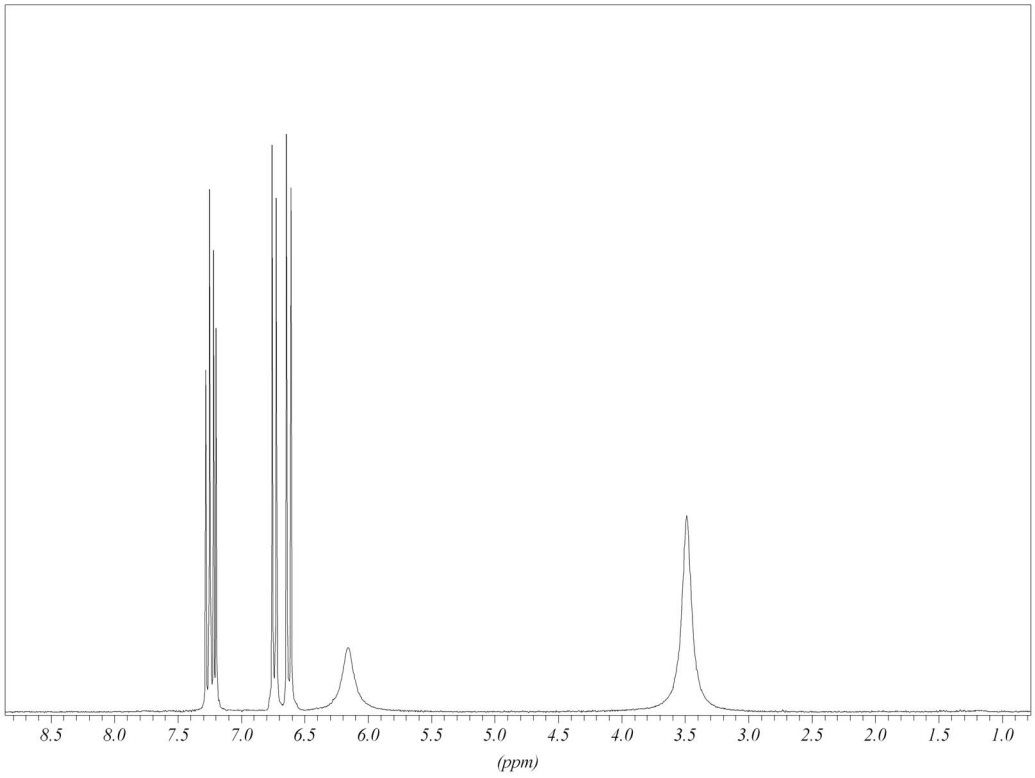

Figure S6. ^{13}C NMR (DMSO-d_6, 63 MHz, 298 K, 2000 scans) of 2-bromo-6-hydrazinopyridine (14)

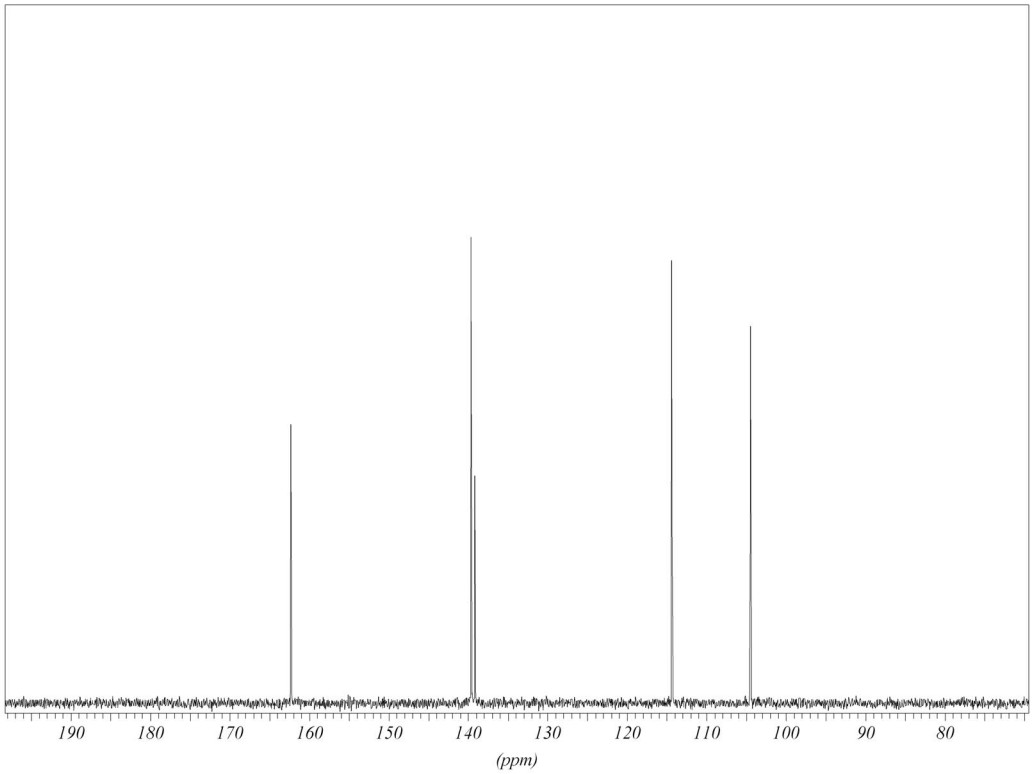

Figure S7. ^{1}H NMR (DMSO-d_6, 250 MHz, 298 K, 16 scans) of 4-iodo-pyrazole (24). Note the signal (~6.2 ppm) coming from a ~3% of pyrazole impurity (starting material) collected in the crystals of **24**.

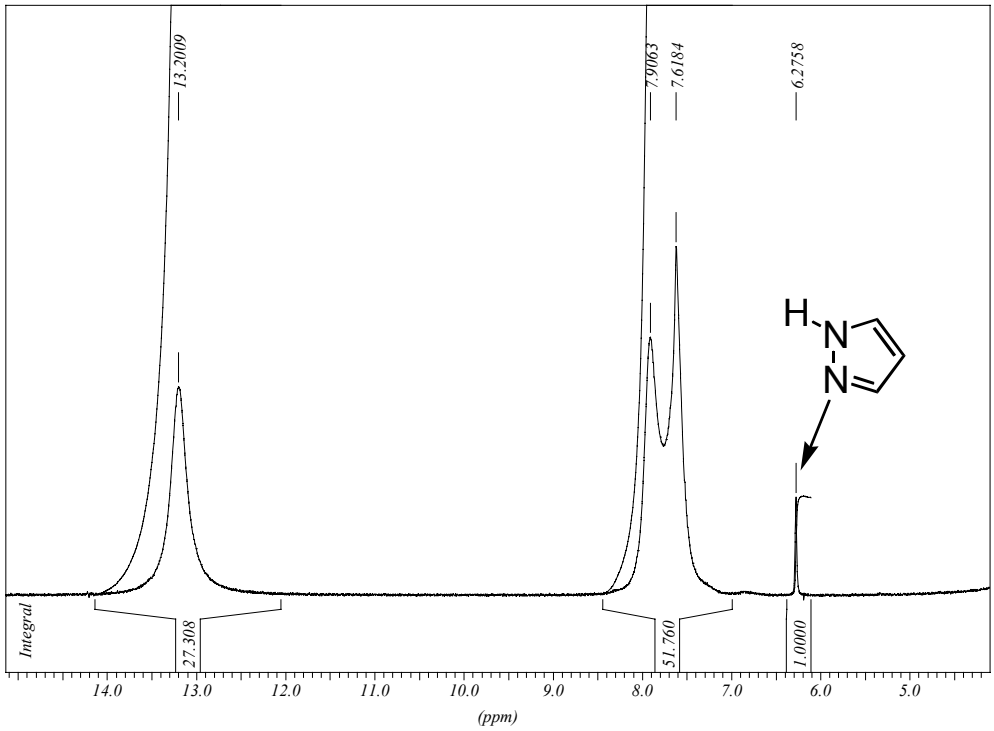

Figure S8. ^{1}H NMR ($CDCl_3$, 250 MHz, 298 K, 32 scans) of 1-(1-ethoxyethyl)-4-Iodo-pyrazole (25).

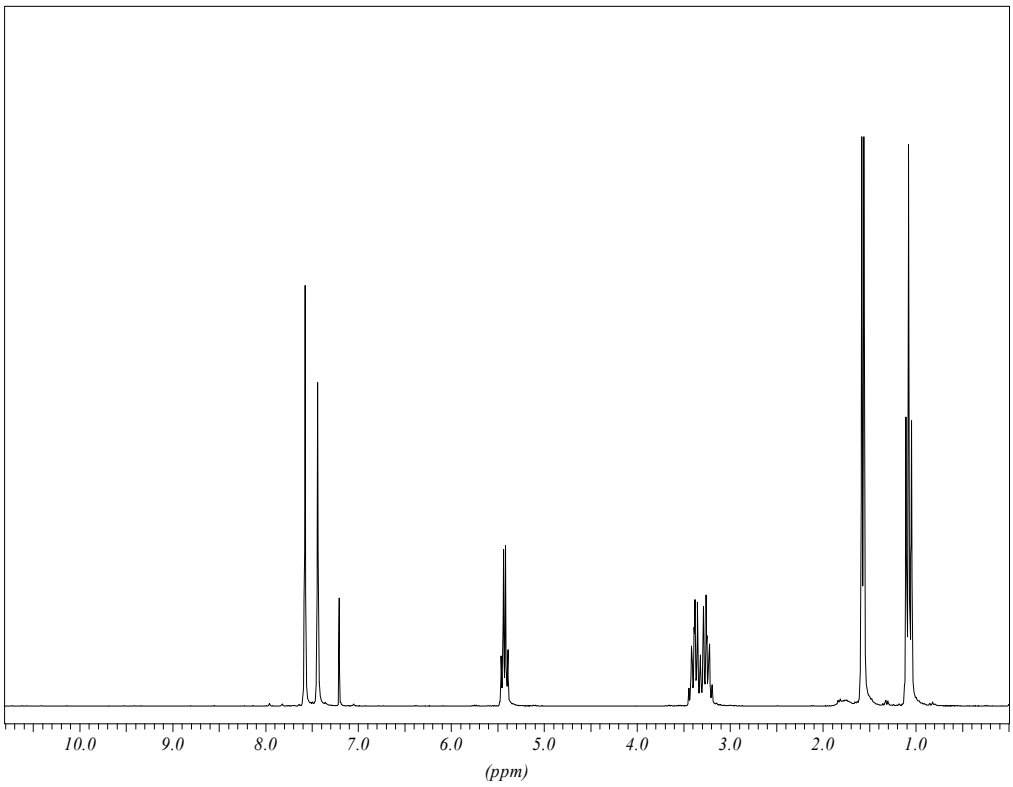

Figure S9. ^{1}H NMR (DMSO-d_6, 250 MHz, 298 K, 32 scans) of 4-formyl-1(H)-pyrazole (26)

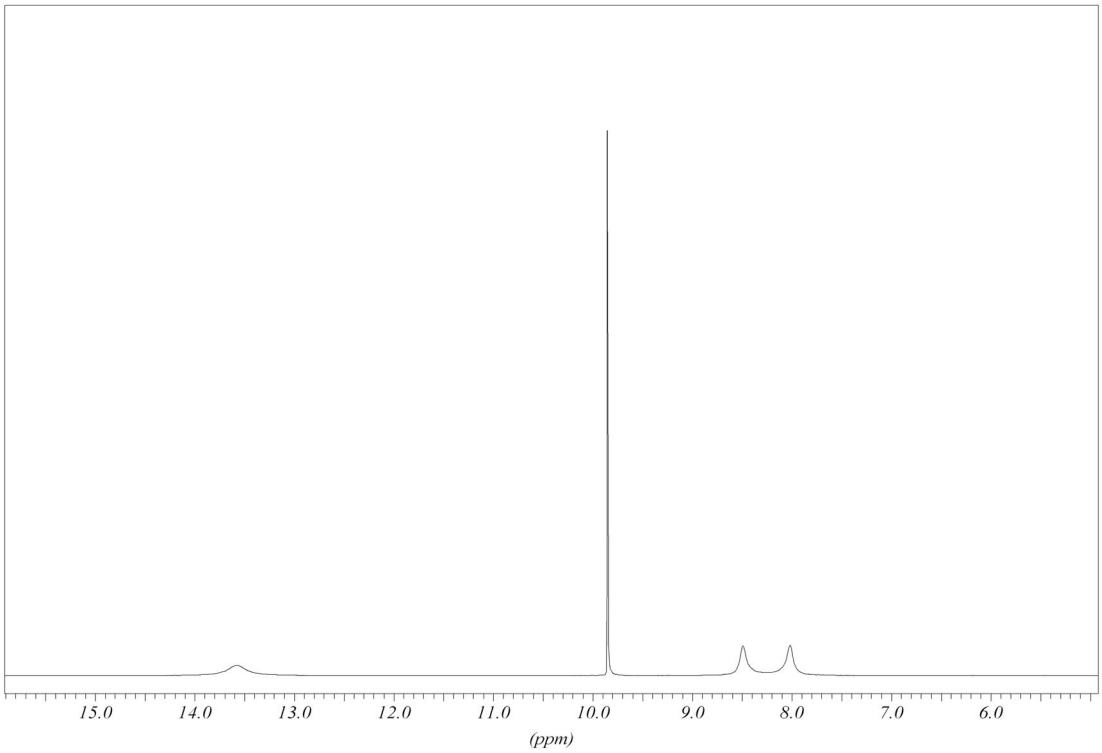

Figure S10. ^{13}C NMR (DMSO-d_6, 63 MHz, 298 K, 6000 scans) of 4-formyl-1(H)-pyrazole (26).

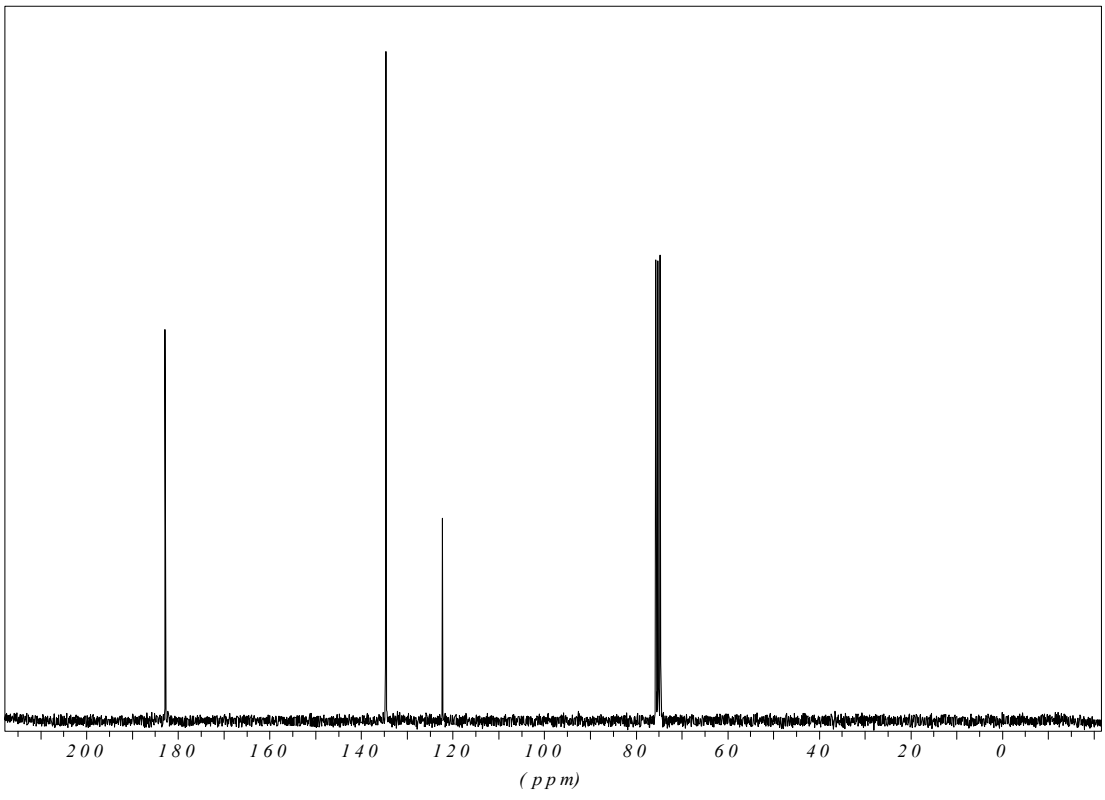

Figure S11. ^{1}H NMR (DMSO-d_6, 250 MHz, 298 K, 16 scans) of 6-bromo-2-[4'-formylpyrazol-1'-yl]-pyridine (7)

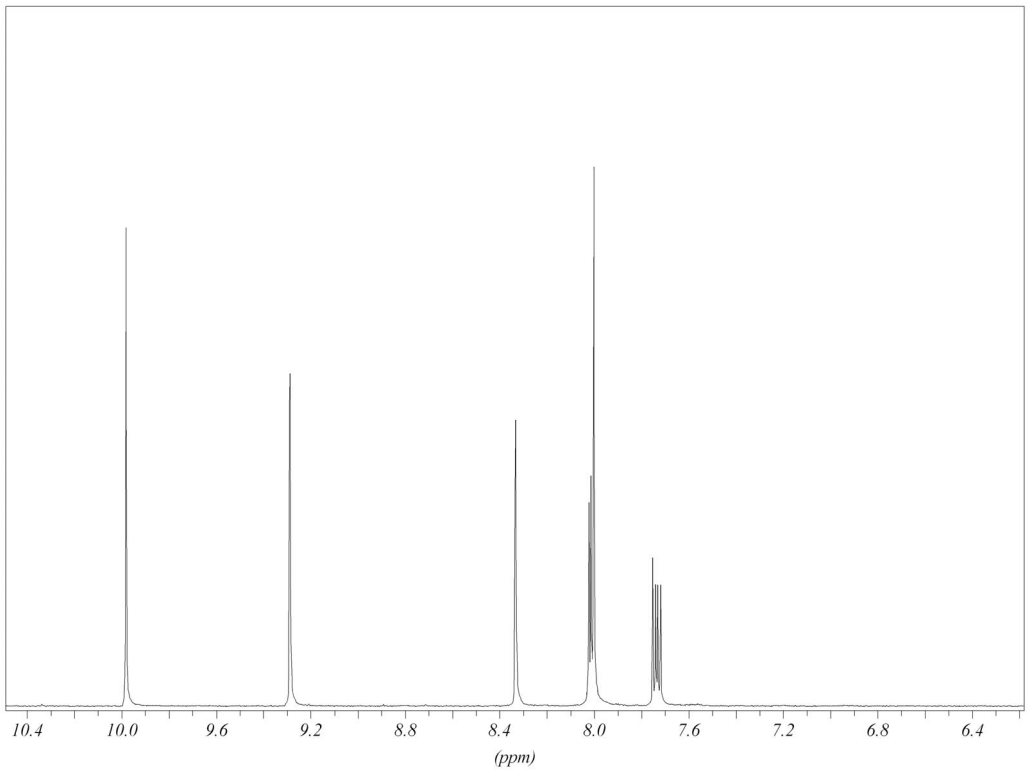

Figure S12. ^{13}C NMR (DMSO-d_6, 63 MHz, 298 K, 1024 scans) of 6-bromo-2-[4'-formylpyrazol-1'-yl]-pyridine (7)

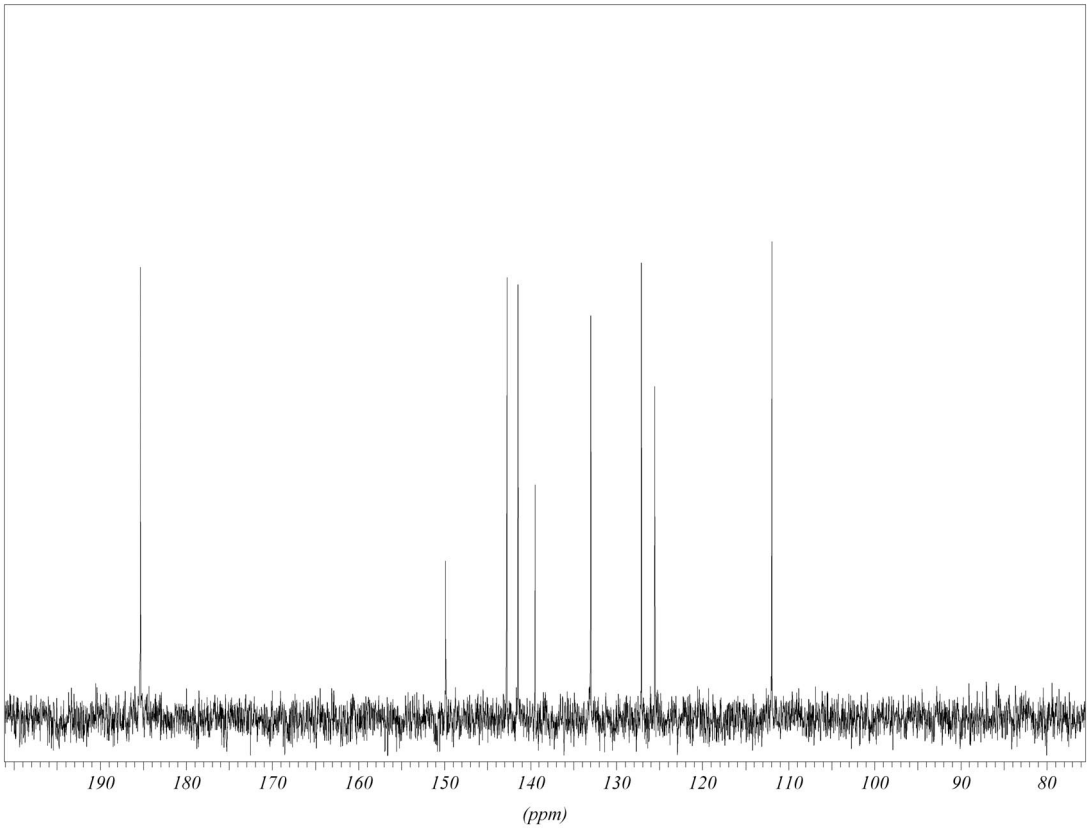

Figure S13. ^{1}H NMR (DMSO-d_6, 250 MHz, 298 K, 64 scans) of 4'',5'-diformyl-6-(pyrazol-1''-yl)-2,2'-bipyridine (9)

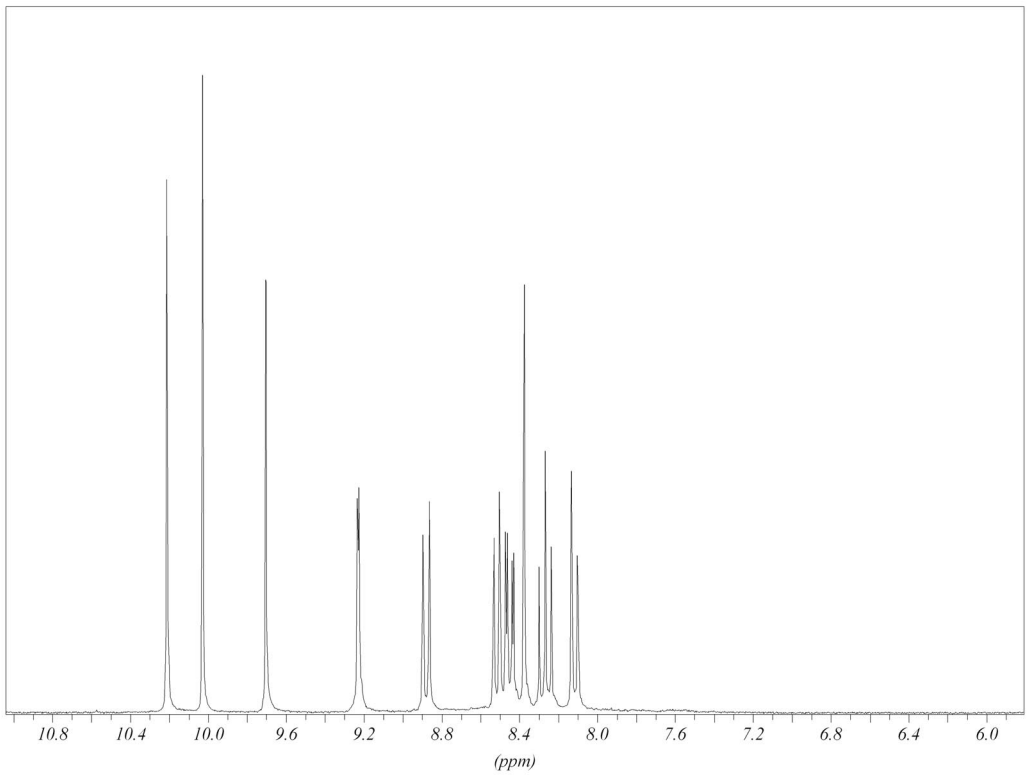

Figure S14. ^{13}C NMR (DMSO-d_6, 63 MHz, 298 K, 8000 scans) of 4'',5'-diformyl-6-(pyrazol-1''-yl)-2,2'-bipyridine (9)

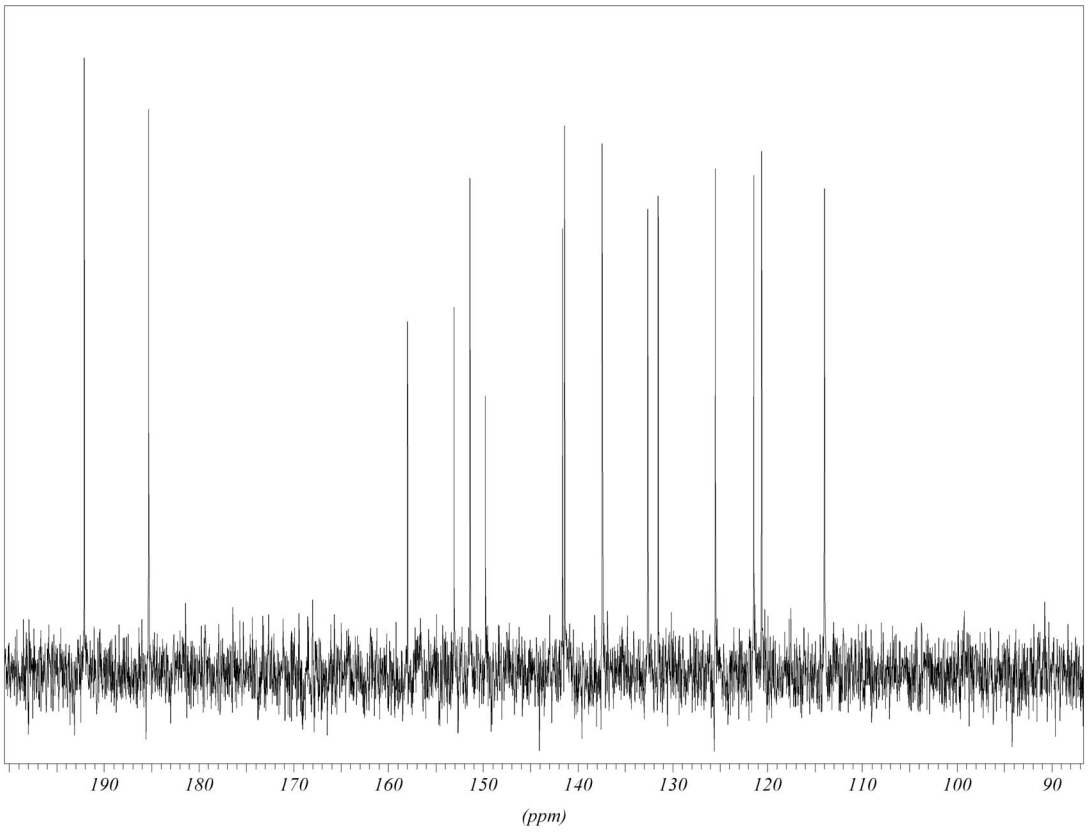

Figure S15. ^{1}H NMR ($CDCl_3$, 250 MHz, 298 K, 16 scans) of 6-bromo-2,2'-dipyridine-5'-carbaldehyde (18)

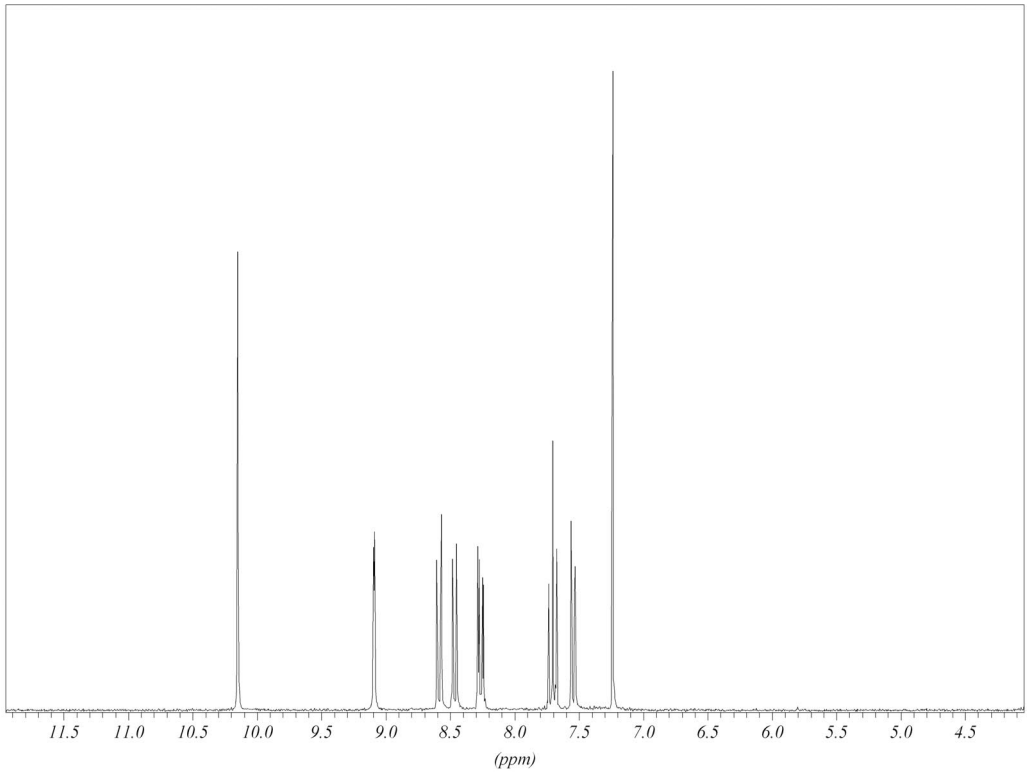

Figure S16. ^{13}C NMR (DMSO-d_6, 63 MHz, 298 K, 9000 scans) of 6-bromo-2,2'-dipyridine-5'-carbaldehyde (18)

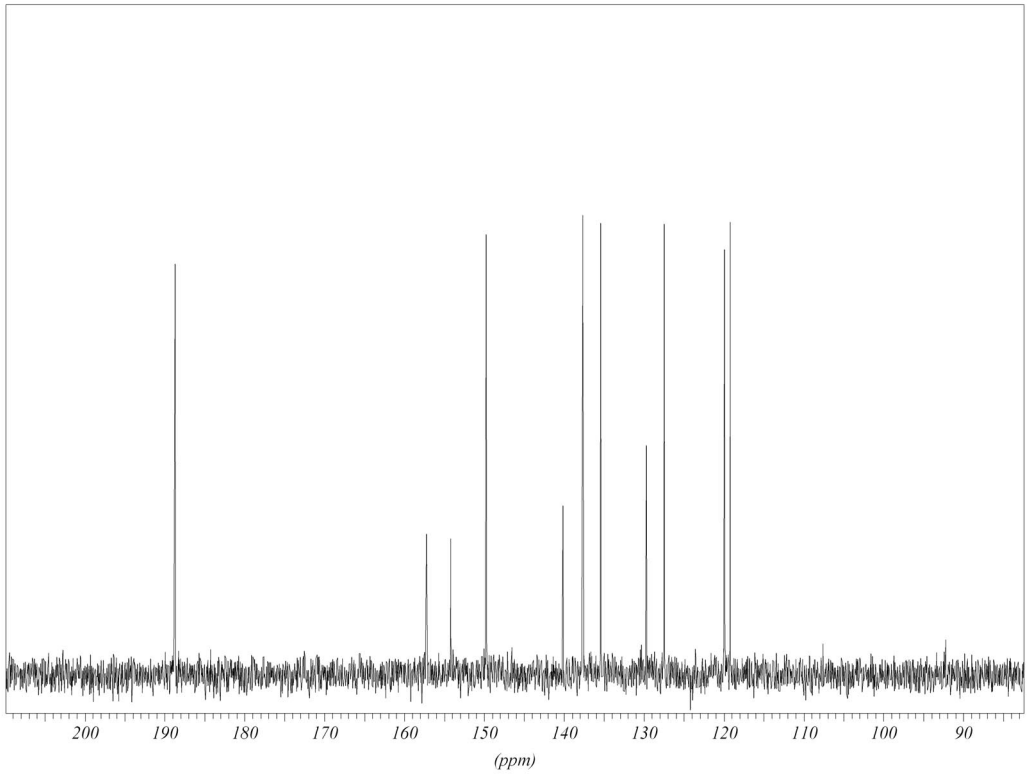

Figure S17. ^{1}H NMR (DMSO-d_6, 250 MHz, 298 K, 64 scans) of 6-bromo-5'[1,3-dihydroxy-4,4,5,5-tetramethyl-imidazolidin-2-yl]-2,2'-bipyridine (19)

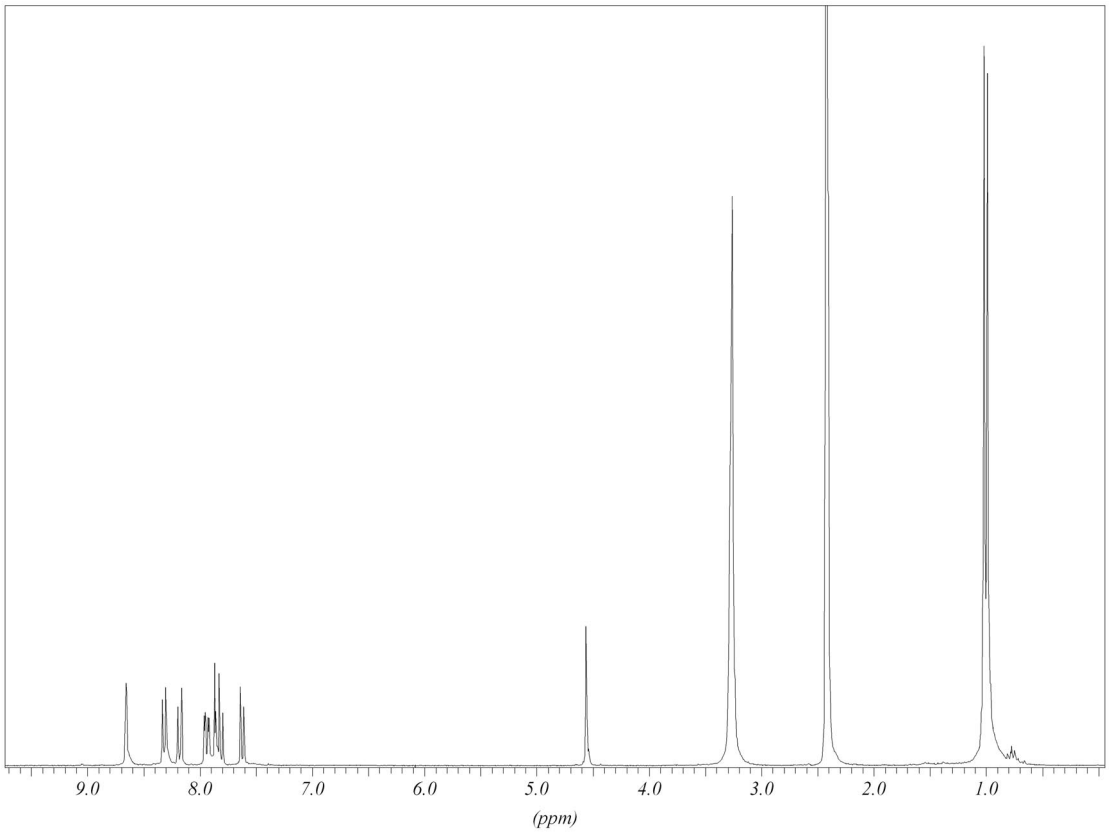

Figure S18. ^{13}C NMR (DMSO-d_6, 63 MHz, 298 K, 9000 scans) of 6-bromo-5'[1,3-dihydroxy-4,4,5,5-tetramethyl-imidazolidin-2-yl]-2,2'-bipyridine (19)

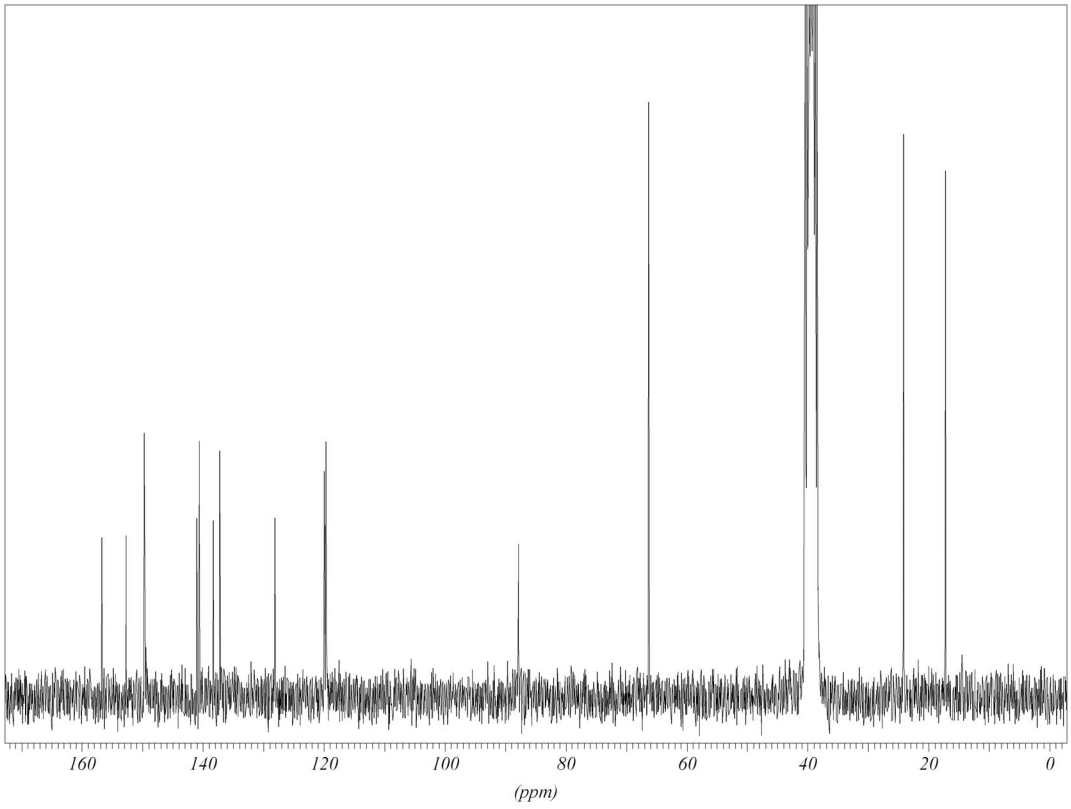

Figure S19A. UV-Vis spectra of **1** (blue line) and **2** (red line) recorded in toluene solutions at room temperature. The inset shows magnified the visible region of the spectra. Note that the transition at 373 nm ($\pi \rightarrow \pi^*$, ε = 17510 $M^{-1} \times cm^{-1}$) originates from the radical connected to the pyrazole ring while that at 392 nm ($\pi \rightarrow \pi^*$, ε =10685 $M^{-1} \times cm^{-1}$) originates from the radical connected to the pyridine ring.

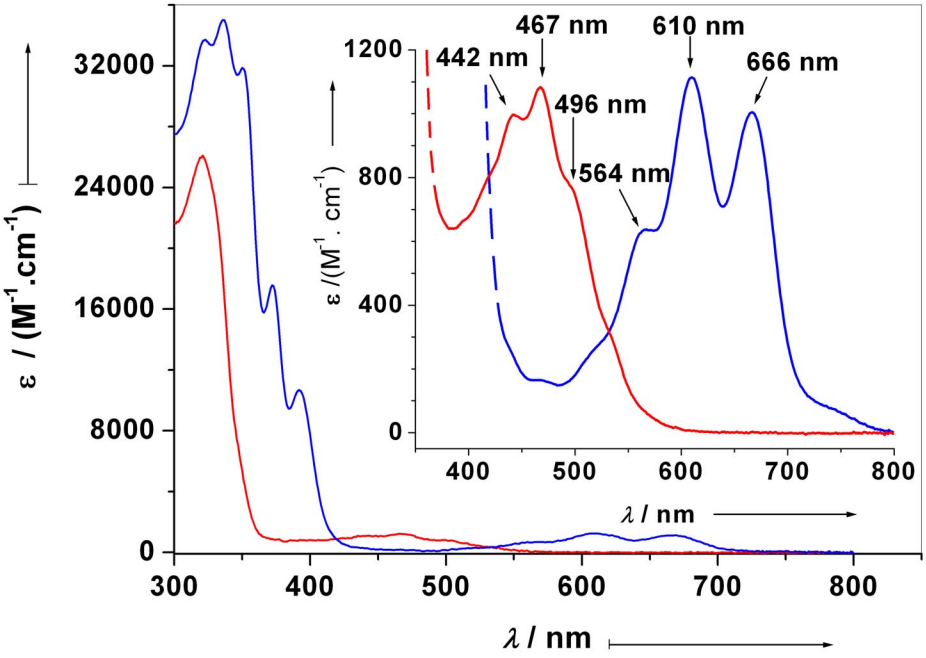

Figure S19B. Comparison of the nitronylnitroxide UV-Vis spectra for the terpyridine biradical **3** (Reference 4, blue line), the bispyrazolylpyridine biradical (olive line, Reference 5), the biradical **1** (violet line) and the monoradical **20** (green line) showing hampered optical properties in the visible region when the NN radical units are directly connected to the pyridine ring.

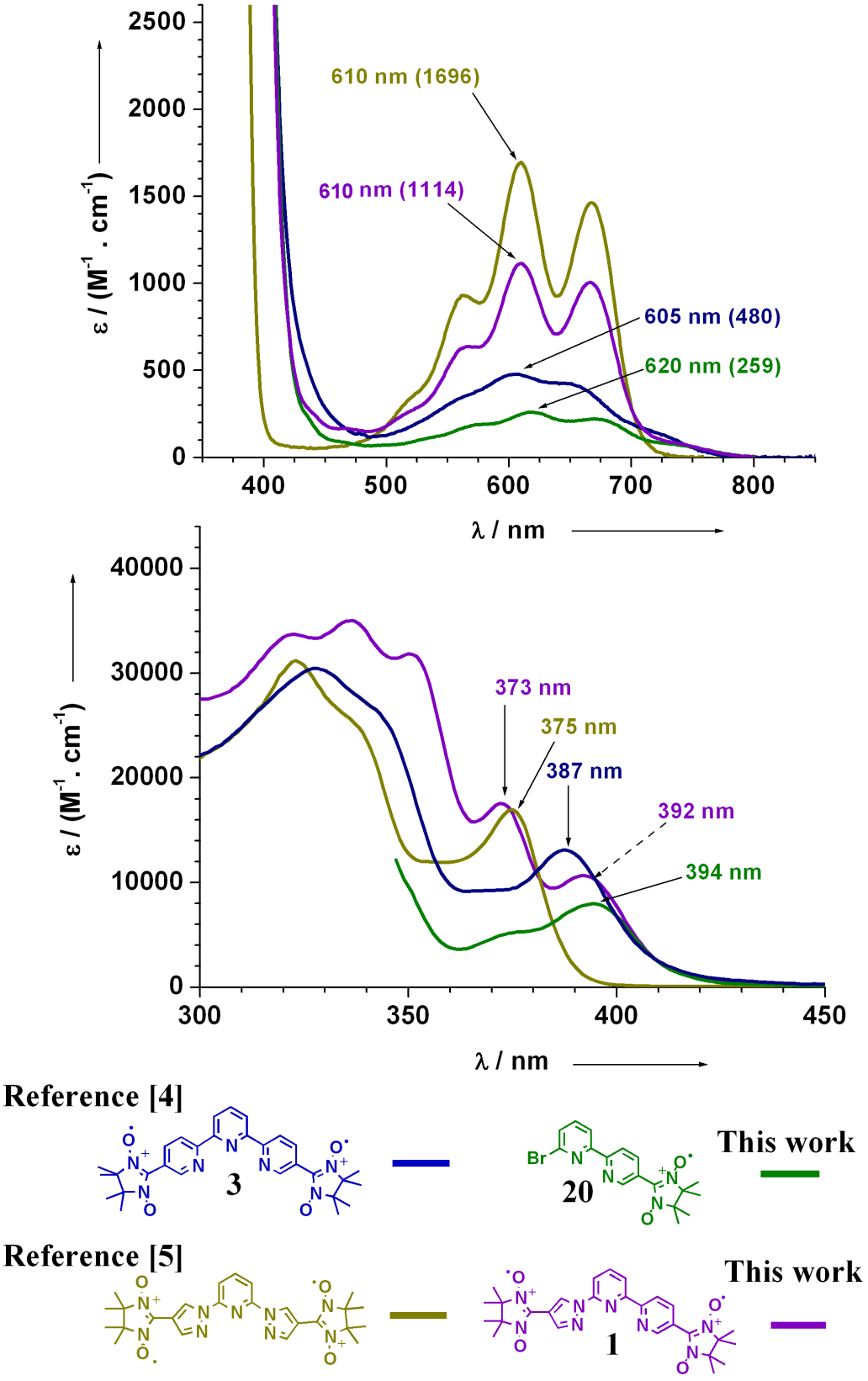

Figure S20. (A) FT-IR spectra recorded in KBr pellet at room temperature for the carbaldeyde (**9**), the radical precursor (**17**), the nitronylnitroxide biradical (**1**) and the iminonitroxide biradical (**2**). Note the asymmetric C=O peak coming from the two different carbaldehyde groups (one connected to the pyridine and the other to the pyrazole moiety). (B) FT-IR spectra recorded in KBr pellet at room temperature of monoradicals **20** (blue line) and **21** (red line).

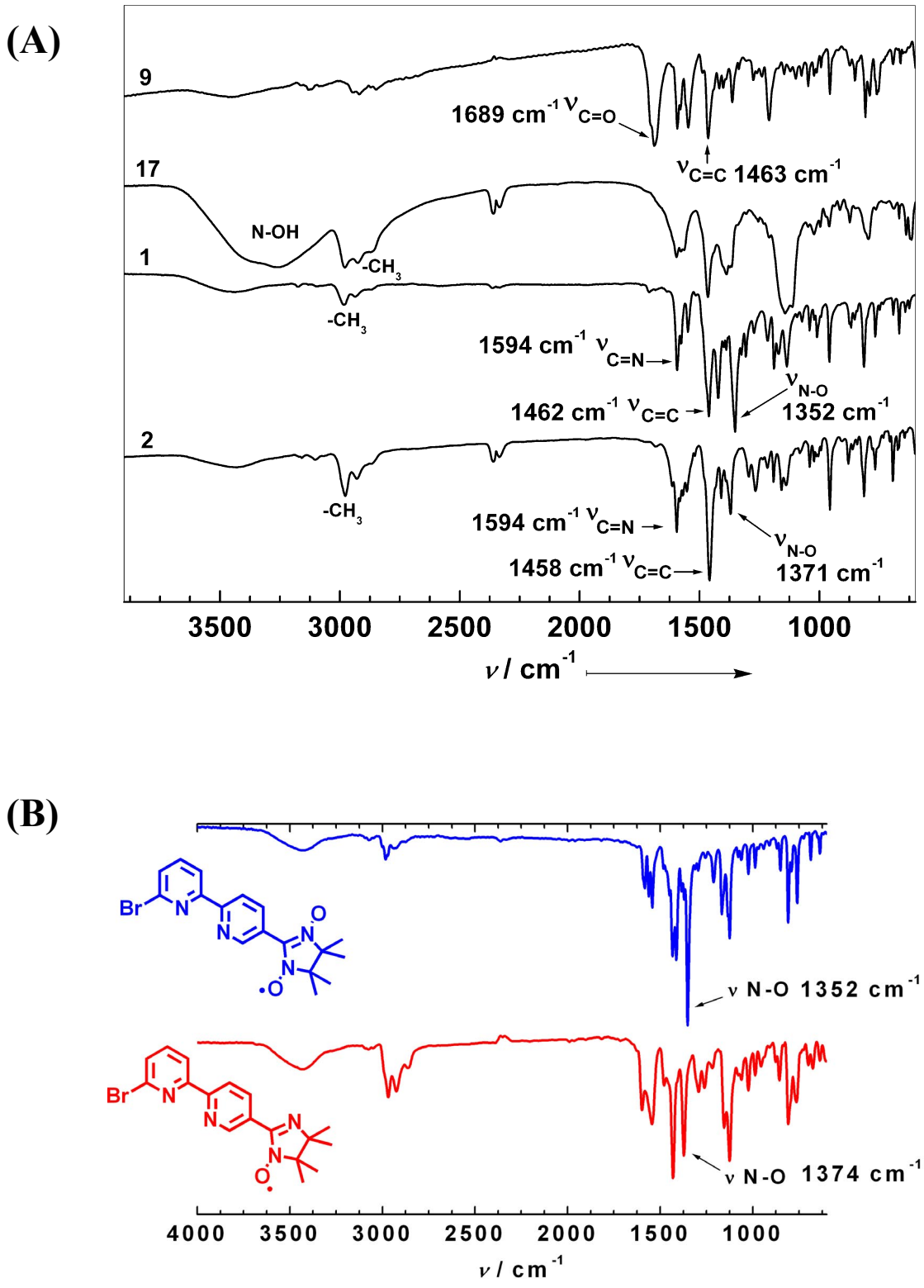

Figure S21. EPR spectrum for the nitronylnitroxide monoradical **20** recorded in toluene solution at 293 K with concentrations of 8×10^{-5} M. Experimental parameters: 9.399870 GHz, 100 kHz modulation frequency, 0.03 mT, 21 msec time constant, 42 sec sweep time, 2.0 mW microwave power, 10^5 gain, 4 scan were accumulated and averaged. The dashed-dotted line (-.-.-) represents the computer simulation with parameters given in **Table 1** (Page S29). The high resolution EPR line marked here with an asterisk is shown in **Figure S22**.

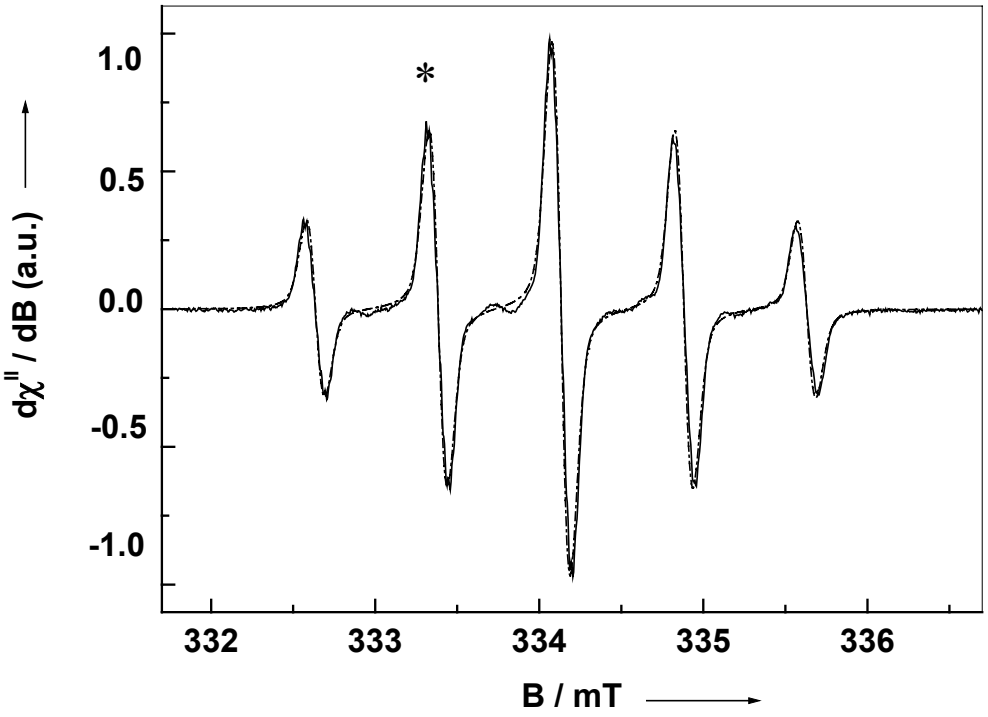

Figure S22. The high resolution EPR spectrum of **20** (blue line, 8×10^{-5} M in toluene) for the M_I = -1 line (marked with an asterisk (*) in Figure S21), recorded with following parameters: 9.39759 GHz, 100 kHz modulation frequency, 0.01 mT modulation amplitude, 41 msec time constant, 84 sec sweep time, 0.8 mW microwave power, 8×10^4 gain, temperature 293 K, 10 scan were accumulated and averaged. The other lines represent the computer simulations with parameters given in **Table 1**.

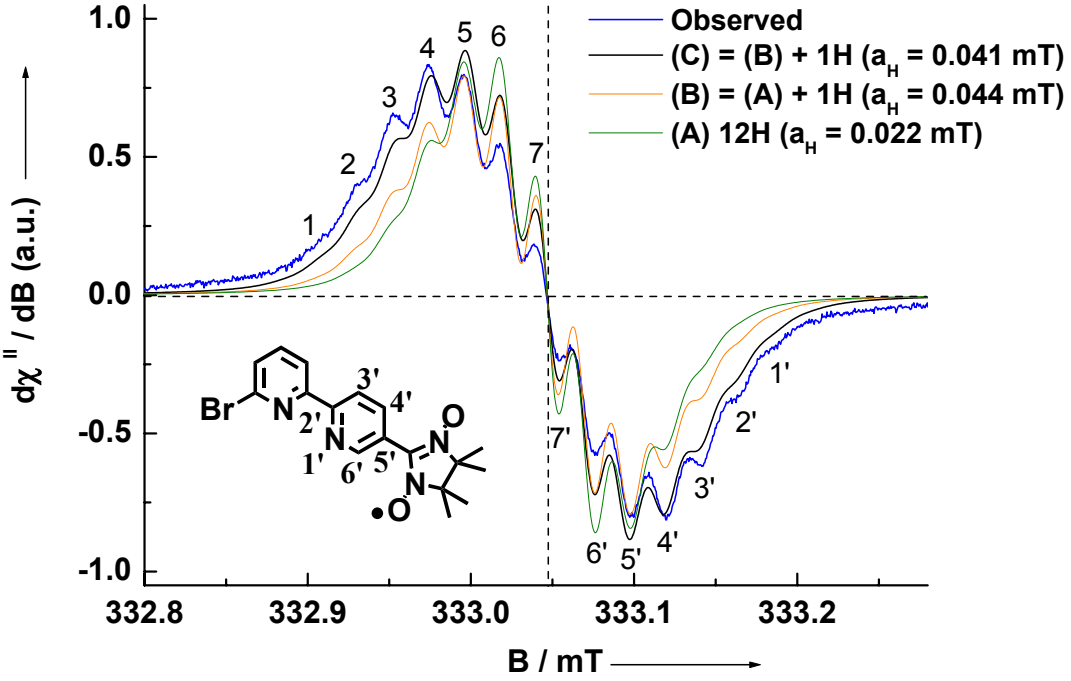

Table 1. Parameters used for the EPR spectrum simulation with N-*hfc* and H-*hfc* as shown in Figure S21 and Figure S22, corresponding to the monoradical **20**.

g_{iso}	2 N	12 H type 3 (-CH_3)	1 H type 2 6'-H	1 H type 1 4'-H	Line-width ΔB_{pp} (mT) §L/G	Simulation
2.0066	a_N = 0.748 mT	a_H = 0.022 mT	-	-	0.020 0.333	Green line
2.0066	a_N = 0.748 mT	a_H = 0.022 mT	a_H = 0.044 mT	-	0.020 0.333	Orange line
2.0066	a_N = 0.748 mT	a_H = 0.022 mT	a_H = 0.044 mT	a_H = 0.041 mT	0.020 0.333	Black line

§ L/G = Lorentzian/Gaussian ratio

Figure S23: EPR spectrum for the monoradicals **21** recorded in toluene solution at 293 K with concentrations of 10^{-4} M. Experimental parameters: 9.40021 GHz, 100 kHz modulation frequency, 0.03 mT modulation amplitude, 21 msec time constant, 42 sec sweep time, 2.0 mW microwave power, 10^5 gain, 4 scan were accumulated and averaged. The dashed-dotted line (-.-.-) corresponds to the computer simulation with parameters: a_{N1} = 0.885 mT, a_{N2} = 0.430 mT, ΔB_{pp} = 0.106 mT.

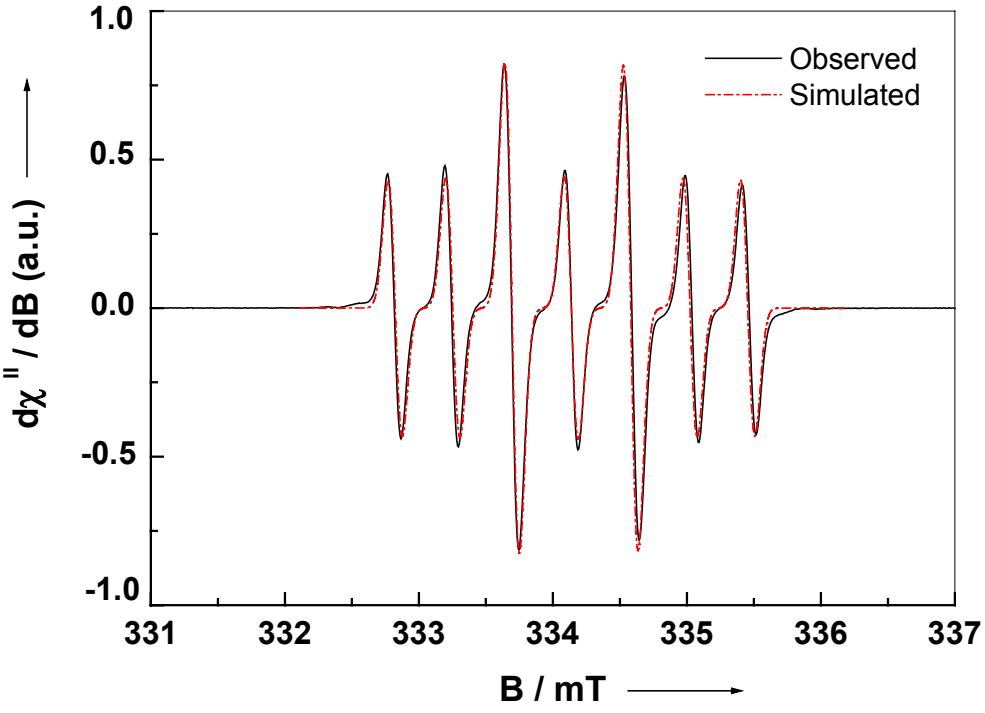

Figure S24. EPR spectrum of **1** (solid blue line)**,** and its computer simulation (dashed black line) recorded in diluted (10^{-4} M) toluene solutions at 293 K. Instrumental parameters: 9.40020 GHz, 100 kHz mod. frequency, 0.03 mT modulation amplitude, 21 msec time constant, 42 sec sweep time, 2.6 mW microwave power, 10^5 gain, 4 scan were accumulated and averaged. The parameters used for the simulation are reported in **Table 2** (Page S33).

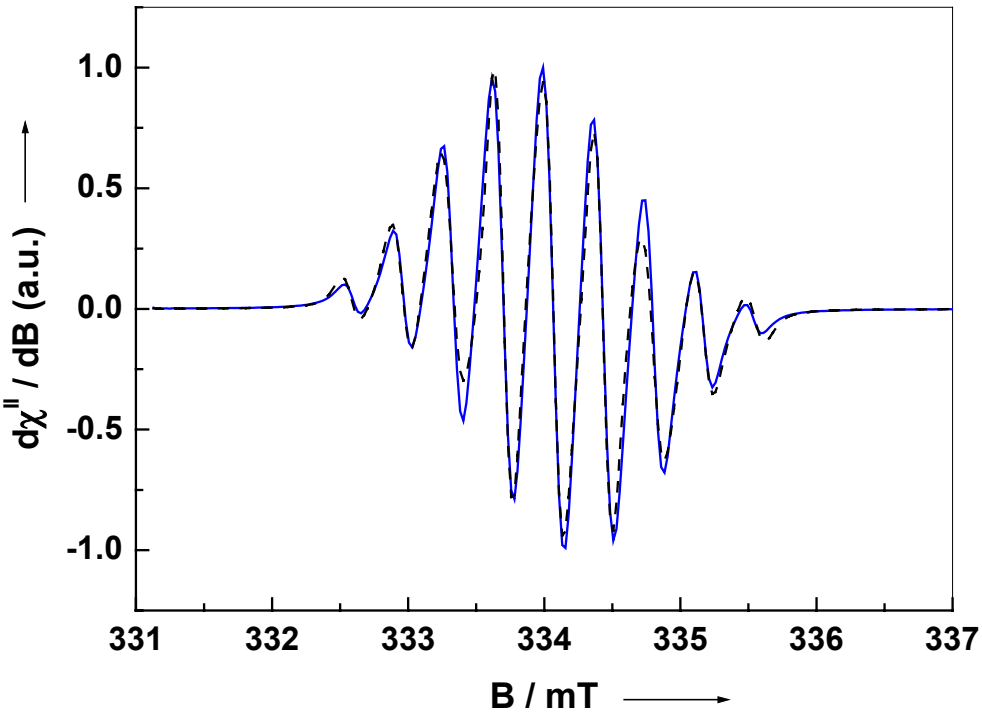

Figure S25. EPR spectrum of **2** (solid red line)**,** and its computer simulation (dashed black line) recorded in diluted (10^{-4} M) toluene solutions at 293 K. Instrumental parameters: 9.40021 GHz, 100 kHz mod. frequency, 0.03 mT modulation amplitude, 21 msec time constant, 42 sec sweep time, 2.6 mW microwave power, 10^5 gain, 4 scan were accumulated and averaged. The parameters used for the simulation are reported in **Table 2** (Page S33).

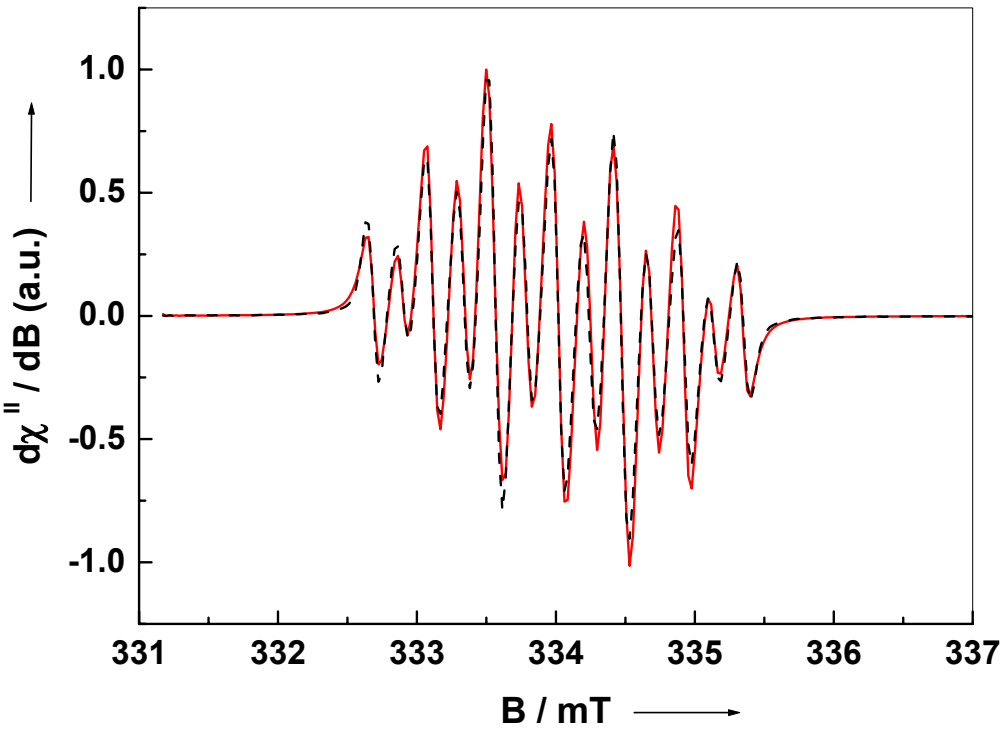

Table 2: Simulation parameters for the biradical **1** and **2** of the r.t. solution EPR spectra (see **Figure S24** for **1** and **Figure S25** for **2**) obtained by numerical diagonalization of the spin-Hamiltonian $\hat{H}$ ‡

	g_{iso}	$\|2J/k_b\|$	$\|a_{N1}\|_{iso}$	$\|a_{N2}\|_{iso}$	Gaussian line-width	Modulation amplitude	rms
1 (NN)	2.0066(1)	≥ 0.069 cm^{-1}	6.876×10^{-4} cm^{-1}	-	1.065×10^{-4} cm^{-1}	2.802×10^{-5} cm^{-1}	≤ 0.806
2 (IN)	2.0061(1)	≥ 0.061 cm^{-1}	3.896×10^{-4} cm^{-1}	8.530×10^{-4} cm^{-1}	7.393×10^{-5} cm^{-1}	2.802×10^{-5} cm^{-1}	≤ 0.696

‡ $\hat{H} = g\beta_e B(\hat{S}_a+\hat{S}_b) - 2J\hat{S}_a\hat{S}_b + \sum_i a_{Ni} \times (\hat{S}_a\hat{I}_{Ni} + \hat{S}_b\hat{I}_{Ni})$

Note: The ESR linewidth is determined by the fluctuation of the (t)-dependent exchange interaction $J(t)$ around its time averaged $\langle J \rangle$, while the resonance positions of each line are determined mainly by $\langle J \rangle$. Thus, if the time dependent term is considered, the exchange term in the spin-Hamiltonian from $-2J\hat{S}_a\hat{S}_b$ has to be changed into $2 \sum_{a,b} [J_{a,b}(t) - \langle J_{a,b} \rangle] \hat{S}_a\hat{S}_b$.

Figure S26. EPR spectra of the Δm_s=1 transitions for **20** (**a,** g_{zz} = 2.0028, $g_{yy} = g_{xx}$ = 2.0086, a_{zz} = 1.8 mT, $a_{yy} = a_{xx}$ = 0.22 mT), **21** (**b,** g_{av} = 2.0061), **1** (**c,** g_{av} = 2.0066) and **2** (**d,** g_{av} = 2.0061) in frozen toluene solutions. Parameters for (**a**) and (**b**): 9.4058 GHz (**a**), and 9.4067 GHz (**b**), then 100 kHz modulation frequency, 0.06 mT modulation amplitude, 41 msec time constant, 42 sec sweep time, 80 μWatt microwave power, temperature 120 K, 4 scan were accumulated and averaged. Parameters for (**c**) and (**d**): 9.4065 GHz (**c**), and 9.4027 GHz (**d**), then 100 kHz modulation frequency, 0.06 mT modulation amplitude, 41 msec time constant, 42 sec sweep time, 200 μWatt microwave power, temperature 120 K, 4 scan were accumulated and averaged. The correspondent Δm_s=2 transitions for **1**and **2** are shown in the inset (**e,** g_{av} ~ 4.01, peak-to-peak line width ΔB_{pp} ~1.1 mT) and (**f,** g_{av} ~ 4.01, ΔB_{pp} ~ 1.1 mT) respectively, recorded at 32 mWatt power, 0.4 mT modulation amplitude, where 32 scan for (**e**) and 26 for (**f**) have been accumulated and averaged. The other parameters were kept the same as the recorded Δm_s=1 transitions.

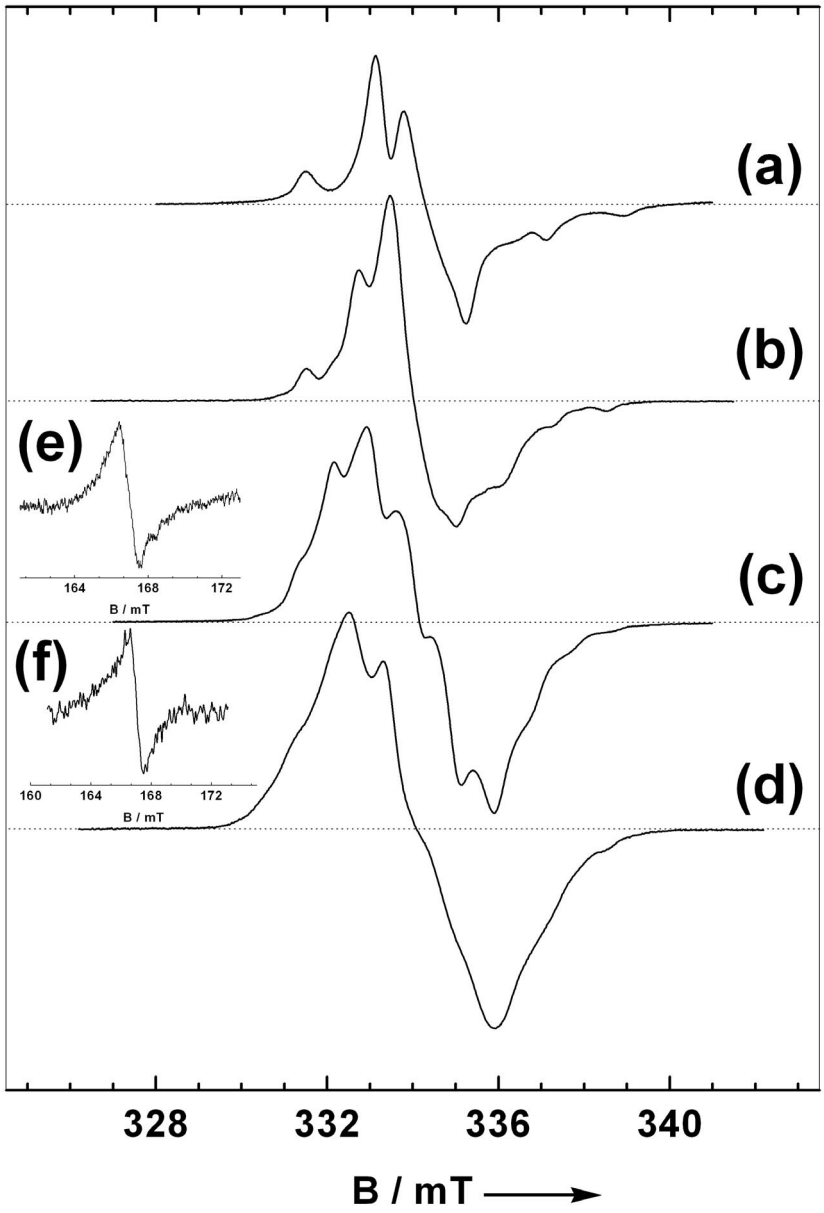

Figure S27. The power saturation behavior of the radicals **20** (●), **21** (●), **1** (■), **2** (■), **3** (▲) and **4** (▲) showing the evolution of the double integrated (DI) signal intensities for the $\Delta m_s=1$ transitions against the root of the power ($P^{1/2}$) in function of the applied microwave power (P) at 122 K, expressed in logarithmic form[§] and normalized ($DI_0/P^{1/2}{}_0$). The solid lines represent the fitting of the experimental data with parameters as follows: **20** (plain line simulation with $P_{1/2}$ = 706.7 ± 39.0 μW, b = 1.048 ± 0.013, R^2 > 0.999), **21** (plain line simulation with $P_{1/2}$ = 1055.8 ± 102.8 μW, b = 1.017 ± 0.026, R^2 > 0.999), **1** (plain line simulation with $P_{1/2}$ = 1165.1 ± 76.2 μW, b = 0.802 ± 0.014, R^2 > 0.999), **2** (plain line simulation with $P_{1/2}$ = 1248.300 ± 79.500 μW, b = 0.918 ± 0.016, R^2 > 0.999), **3** (plain line simulation with $P_{1/2}$ = 612.7 ± 187.8 μW, b = 0.287 ± 0.09, R^2 > 0.991), and **4** (plain line simulation with $P_{1/2}$ = 1411.8 ± 126.9 μW, b = 1.217 ± 0.031, R^2 > 0.999).

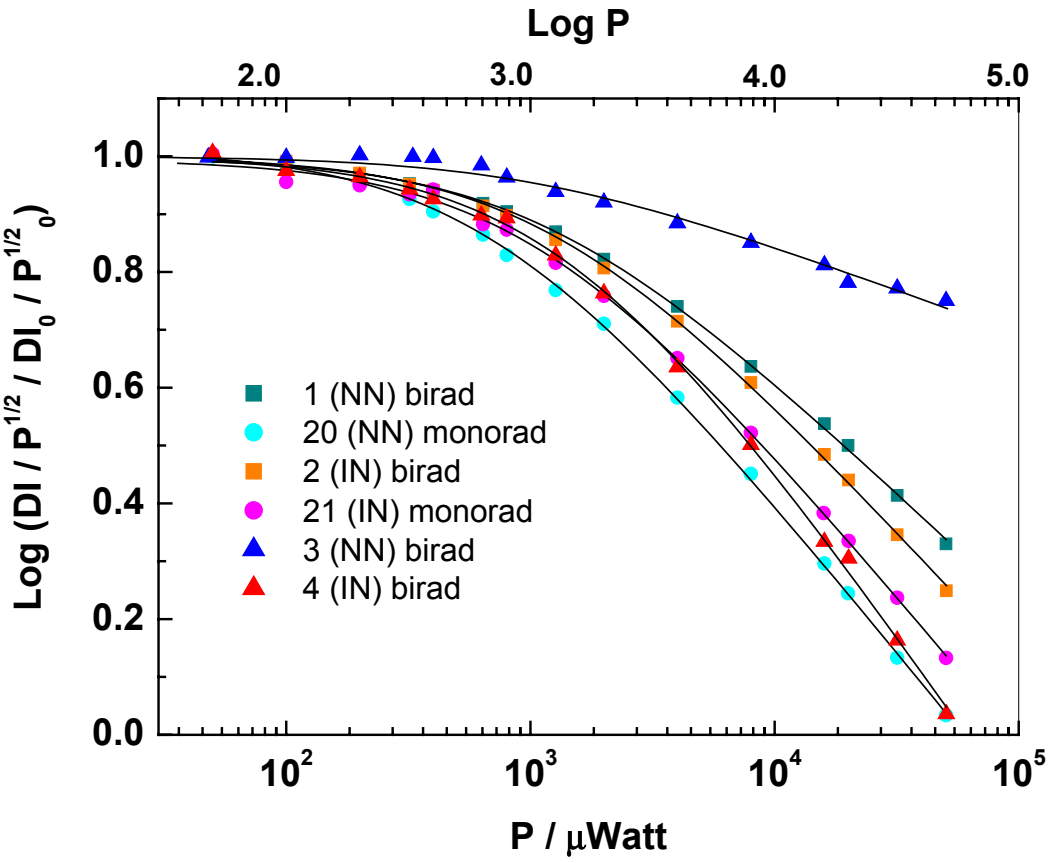

[§]The equation applied in the fitting was: Log_{10} (DI / √ P) = Log_{10} *k* – (b/2) Log_{10} [1 + (P / $P_{1/2}$)]

Figure S28. (A) The Curie plot of the iminonitroxide biradical **2** [10^{-3} M in toluene]. The DI indicates the double integrated signal intensity of the forbidden half-field transition. The inset shows the forbidden half-field transition recorded at 4.2 K. **(B)** The product DI × T *versus* T. The solid red line corresponds to the best fitting of the data according to the Bleaney-Bowers model for two interacting S=1/2 spin systems assuming triplet (S=1) ground state, and the dashed-dotted magenta line the simulation assuming singlet (S=0) ground state with parameters given in the text.

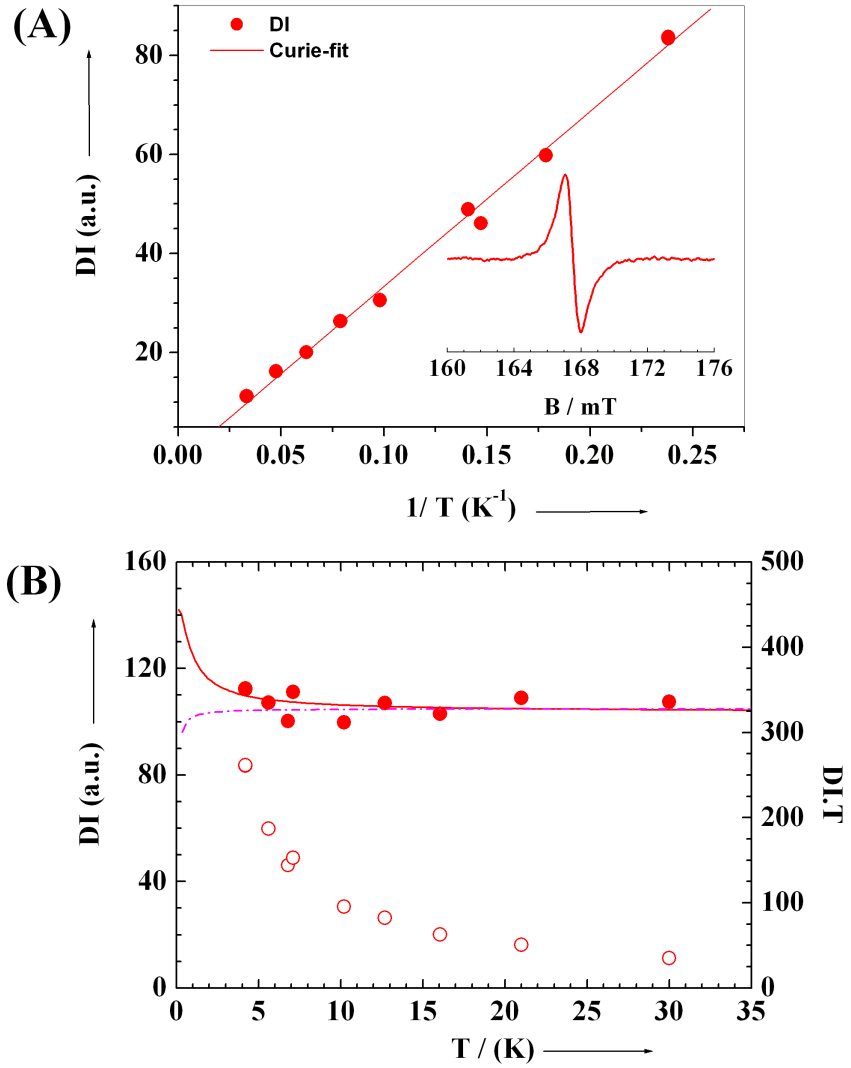

Figure S29. (A) The Curie plot of the nitronylnitroxide biradical based on the terpyridine system **3** [10^{-3} M in toluene]. The DI indicates the double integrated signal intensity of the forbidden half-field transition. The inset shows the forbidden half-field transition recorded at 4.0 K. **(B)** The product DI × T *versus* T. The solid blue line corresponds to the best fitting of the data according to the Bleaney-Bowers model for two interacting S=1/2 spin systems with parameters given in the text.

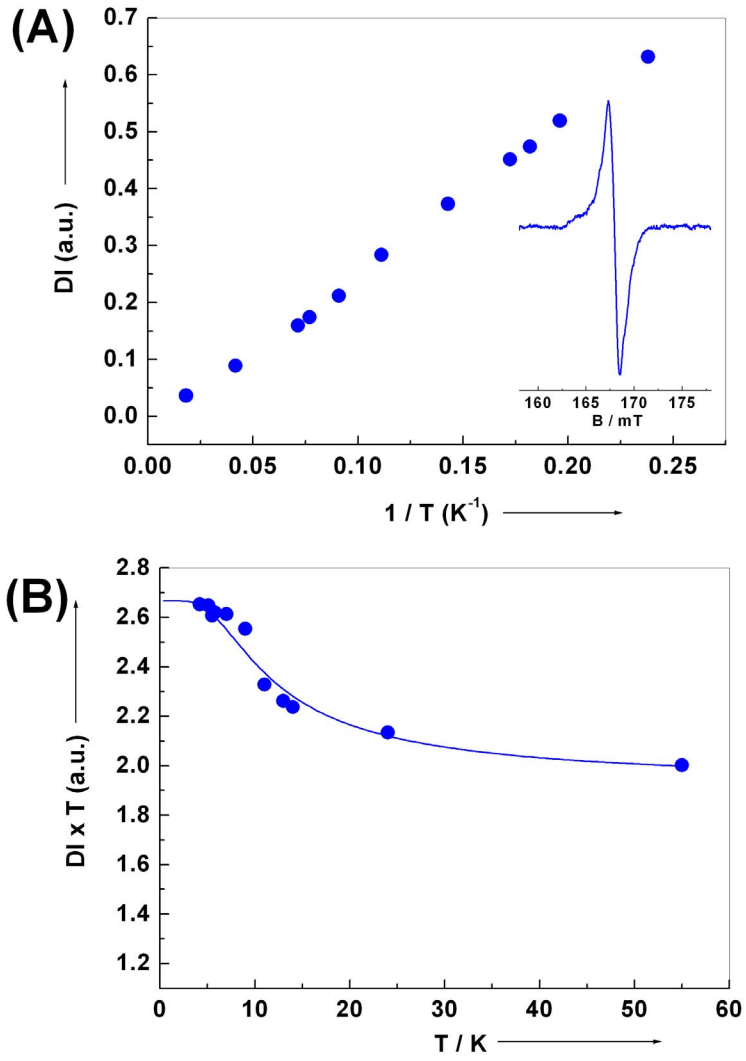

Figure S30. (A) The Curie plot of the iminonitroxide biradical **4** [10^{-3} M in toluene] where DI indicates the double integrated signal intensity of the forbidden half-field transition. The inset shows the forbidden half-field transition recorded at 7.3 K. **(B)** The product DI × T *versus* T. The solid red line corresponds to the best fitting of the data according to the Bleaney-Bowers model for two interacting S=1/2 spin systems with parameters given in the text.

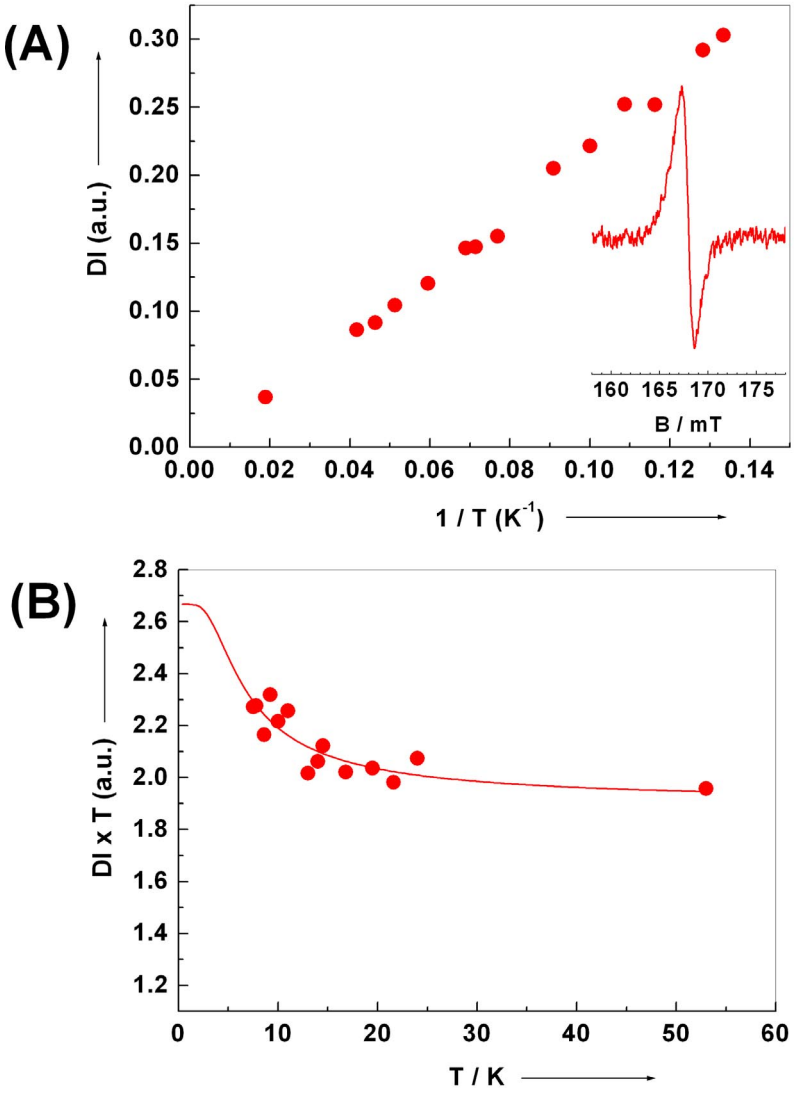

Figure S31. X-ray structure of the monoradical **20** (the standard for spin quantitation for the biradical systems **1**, and **3**) with a perspective of the crystal packing. CCDC number for **20**: 229004. Thermal ellipsoids are drawn at the 50% of the probability level. The hydrogen's atoms were omitted for clarity.

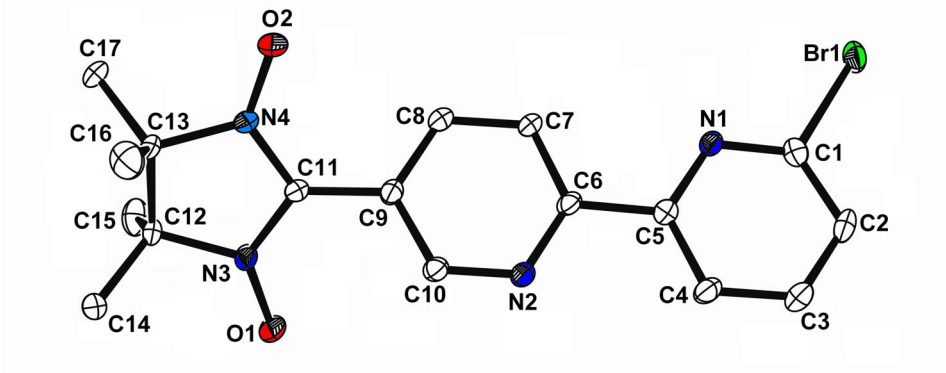

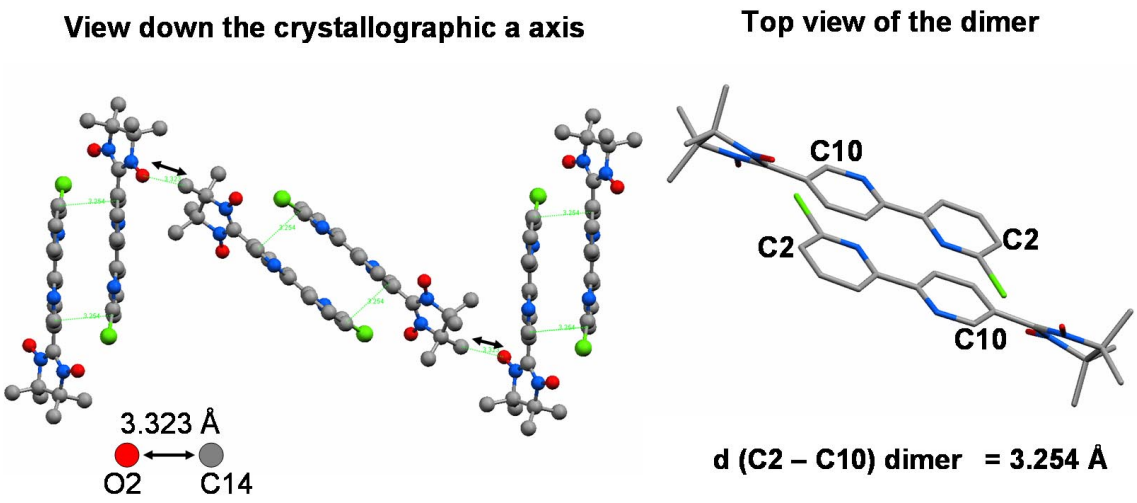

Table 3: X-ray data for **20**, experimental details, structure solutions and refinements.

Compound	**20**
CCDC number	229004
Formula	$C_{17}H_{18}BrN_4O_2$
Formula Weight *M*	390.25
Crystal System	Monoclinic
Space group	$P2_1/n$ (No.14)
a (Å)	6.6600(4)
b (Å)	10.9300(5)
c (Å)	23.1570(7)
α (°)	90
β (°)	96.3620(13)
γ (°)	90
V (Å^3)	1675.31(14)
Z	4
ρ_{calc} (g×cm^{-3})	1.547
μ (MoKα) (mm^{-1})	2.471
F(000)	796
Crystal Size (mm)	0.08×0.15×0.41
Colour	Blue
Shape	Needles
Temperature (K)	120
Radiation, λ(Å)	MoKα,0.71073
θ Min-Max (°)	4.0-29.5
Total data	19655
Unique data	4621
R_{int}	0.000
Observed data	2764
N_{ref}	2764
N_{par}	217
S	1.08
[a] R_1	0.0405
[b] wR_2	0.0448

[a] $R_1 = \sum||F_0| - |F_c||/\sum|F_0|$
[b] $wR_2 = \{\sum w(|F_0| - |F_c|)^2/\sum w|F_0|^2\}^{½}$